



1 **Bias corrections of GOSAT SWIR XCO<sub>2</sub> and XCH<sub>4</sub> with**  
2 **TCCON data and their evaluation using aircraft**  
3 **measurement data**

4

5 **M. Inoue<sup>1,\*</sup>, I. Morino<sup>1</sup>, O. Uchino<sup>1</sup>, T. Nakatsuru<sup>1</sup>, Y. Yoshida<sup>1</sup>, T. Yokota<sup>1</sup>, D.**  
6 **Wunch<sup>2</sup>, P. O. Wennberg<sup>2</sup>, C. M. Roehl<sup>2</sup>, D. W. T. Griffith<sup>3</sup>, V. A. Velazco<sup>3</sup>, N. M.**  
7 **Deutscher<sup>3,4</sup>, T. Warneke<sup>4</sup>, J. Notholt<sup>4</sup>, J. Robinson<sup>5</sup>, V. Sherlock<sup>5,\*\*</sup>, F. Hase<sup>6</sup>, T.**  
8 **Blumenstock<sup>6</sup>, M. Rettinger<sup>7</sup>, R. Sussmann<sup>7</sup>, E. Kyrö<sup>8</sup>, R. Kivi<sup>8</sup>, K. Shiomi<sup>9</sup>, S.**  
9 **Kawakami<sup>9</sup>, M. De Mazière<sup>10</sup>, S. G. Arnold<sup>11</sup>, D. G. Feist<sup>11</sup>, E. A. Barrow<sup>12</sup>, J.**  
10 **Barney<sup>12</sup>, M. Dubey<sup>13</sup>, M. Schneider<sup>6</sup>, L. Iraci<sup>14</sup>, J. R. Podolske<sup>14</sup>, P. Hillyard<sup>14,15</sup>,**  
11 **T. Machida<sup>1</sup>, Y. Sawa<sup>16</sup>, K. Tsuboi<sup>16</sup>, H. Matsueda<sup>16</sup>, C. Sweeney<sup>17</sup>, P. P. Tans<sup>17</sup>,**  
12 **A. E. Andrews<sup>17</sup>, S. C. Biraud<sup>18</sup>, Y. Fukuyama<sup>19</sup>, J. V. Pittman<sup>20</sup>, E. A. Kort<sup>21,2,\*\*\*</sup>,**  
13 **and T. Tanaka<sup>1,9,\*\*\*\*</sup>**

14

15 [1]{National Institute for Environmental Studies (NIES), Tsukuba, Japan}

16 [2]{California Institute for Technology, Pasadena, CA, USA}

17 [3]{Centre for Atmospheric Chemistry, University of Wollongong, New South Wales,  
18 Australia}

19 [4]{Institute of Environmental Physics, University of Bremen, Bremen, Germany}

20 [5]{National Institute of Water and Atmospheric Research, Lauder, New Zealand}

21 [6]{IMK-ASF, Karlsruhe Institute of Technology, Karlsruhe, Germany}

22 [7]{IMK-IFU, Karlsruhe Institute of Technology, Garmisch-Partenkirchen, Germany}

23 [8]{Arctic Research Centre, Finnish Meteorological Institute (FMI), Sodankylä, Finland}

24 [9]{Japan Aerospace Exploration Agency (JAXA), Tsukuba, Japan}

25 [10]{Belgium Institute for Space Aeronomy (IASB-BIRA), Brussels, Belgium}

26 [11]{Max Planck Institute for Biogeochemistry (MPI-BGC), Jena, Germany}

27 [12]{Ivy Tech Community College of Indiana, Indianapolis, IN, USA}



- 1 [13]{Los Alamos National Laboratory, Los Alamos, NM, USA}  
2 [14]{NASA Ames Research Center, Moffett Field, CA, USA}  
3 [15]{Bay Area Environmental Research Institute, Petaluma, CA, USA}  
4 [16]{Meteorological Research Institute (MRI), Tsukuba, Japan}  
5 [17]{National Oceanic and Atmospheric Administration (NOAA), Boulder, CO, USA}  
6 [18]{Lawrence Berkeley National Laboratory (LBNL), Berkeley, CA, USA}  
7 [19]{Japan Meteorological Agency, Tokyo, Japan}  
8 [20]{Department of Earth and Planetary Sciences, Harvard University, Cambridge, MA,  
9 USA}  
10 [21]{Jet Propulsion Laboratory, Pasadena, CA, USA}  
11  
12 [\*] {now at: Department of Biological Environment, Akita Prefectural University, Akita,  
13 Japan}  
14 [\*\*] {now at: Laboratoire de Météorologie Dynamique, Palaiseau, France}  
15 [\*\*\*] {now at: Department of Atmospheric, Oceanic and Space Sciences, University of  
16 Michigan, Ann Arbor, MI, USA}  
17 [\*\*\*\*] {now at: NASA Ames Research Center, Moffett Field, CA, USA}  
18  
19 Correspondence to: M. Inoue (makoto@akita-pu.ac.jp)

20

## 21 **Abstract**

22

23 We describe a method for removing systematic biases of column-averaged dry air mole  
24 fractions of CO<sub>2</sub> (XCO<sub>2</sub>) and CH<sub>4</sub> (XCH<sub>4</sub>) derived from short-wavelength infrared (SWIR)  
25 spectra of the Greenhouse gases Observing SATellite (GOSAT). We conduct correlation  
26 analyses between the GOSAT biases and simultaneously-retrieved auxiliary parameters. We  
27 use these correlations to bias correct the GOSAT data, removing these spurious correlations.



1 Data from Total Carbon Column Observing Network (TCCON) were used as reference values  
2 for this regression analysis. To evaluate the effectiveness of this correction method, the  
3 uncorrected/corrected GOSAT data were compared to independent XCO<sub>2</sub> and XCH<sub>4</sub> data  
4 derived from aircraft measurements taken for the Comprehensive Observation Network for  
5 TRace gases by AIrLiner (CONTRAIL) project, the National Oceanic and Atmospheric  
6 Administration (NOAA), the U.S. Department of Energy (DOE), the National Institute for  
7 Environmental Studies (NIES), the Japan Meteorological Agency (JMA), the HIAPER Pole-  
8 to-Pole observations (HIPPO) program, and the GOSAT validation aircraft observation  
9 campaign over Japan. These comparisons demonstrate that the empirically-derived bias  
10 correction improves the agreement between GOSAT XCO<sub>2</sub>/XCH<sub>4</sub> and the aircraft data.  
11 Finally, we present latitudinal distributions and temporal variations of the derived GOSAT  
12 biases.

13

## 14 **1 Introduction**

15 Atmospheric carbon dioxide (CO<sub>2</sub>) and methane (CH<sub>4</sub>) are crucially important anthropogenic  
16 greenhouse gases that contribute to global warming and future climate change. The  
17 Greenhouse gases Observing SATellite (GOSAT), launched in January 2009, is the world's  
18 first satellite specialized for measuring the concentrations of atmospheric CO<sub>2</sub> and CH<sub>4</sub> from  
19 space (Yokota et al., 2009). Column-averaged dry air mole fractions of CO<sub>2</sub> (XCO<sub>2</sub>) and CH<sub>4</sub>  
20 (XCH<sub>4</sub>) are retrieved from the Short-Wavelength InfraRed (SWIR) spectra of the Thermal  
21 And Near-infrared Sensor for carbon Observation - Fourier Transform Spectrometer  
22 (TANSO-FTS) onboard GOSAT. Validation of XCO<sub>2</sub> and XCH<sub>4</sub> derived from the GOSAT  
23 TANSO-FTS has been conducted by using ground-based high-resolution Fourier Transform  
24 Spectrometer (ground-based FTS) data and aircraft measurements (Morino et al., 2011; Saitoh  
25 et al., 2012; Yoshida et al., 2013; Inoue et al., 2013, 2014; Gavrilov et al., 2014). The results  
26 showed that the GOSAT SWIR XCO<sub>2</sub> measurements (Ver. 02.00) are biased -1–2 ppm (±1–3  
27 ppm) against the aircraft measurement data (Inoue et al., 2013), whereas GOSAT SWIR  
28 XCH<sub>4</sub> measurements (Ver. 02.00) are biased positively by 2–7 ppb with a standard deviation  
29 of about 15 ppb (Inoue et al., 2014).

30

31 The systematic biases of the GOSAT XCO<sub>2</sub> and XCH<sub>4</sub> retrievals are produced by many  
32 factors including aerosol optical depth, thin cirrus clouds, and surface pressure retrieval error



1 (e.g., Uchino et al., 2012; Yoshida et al., 2013). These biases can lead to large errors in the  
2 estimations of regional fluxes of CO<sub>2</sub> and CH<sub>4</sub> from inversion analyses (Takagi et al., 2011;  
3 Maksyutov et al., 2013; Deng et al., 2014; Ishizawa et al., in preparation). Consequently,  
4 several studies have described bias corrections of the satellite retrieval data by using multiple  
5 linear regression (e.g., Wunch et al., 2011b; Guerlet et al., 2013; Schneising et al., 2013).  
6 Wunch et al. (2011b) have attempted to correct spatially and temporally varying biases in the  
7 Atmospheric CO<sub>2</sub> Observations from Space retrievals of the GOSAT (ACOS-GOSAT;  
8 O'Dell et al., 2012; Crisp et al., 2012) data obtained over land using an empirical linear  
9 regression model with which they correlated variabilities in XCO<sub>2</sub> retrievals with surface  
10 albedo, the difference between the retrieved and a priori surface pressure, airmass, and the  
11 oxygen A-band spectral radiance. They used the GOSAT data in the Southern Hemisphere as  
12 the reference values for the linear regression and evaluated the bias correction against the  
13 Total Carbon Column Observing Network (TCCON) data from the Northern Hemisphere.

14

15 In this study, we develop a method for correcting the systematic biases of the GOSAT XCO<sub>2</sub>  
16 and XCH<sub>4</sub> retrievals (Ver. 02.21) provided by the National Institute for Environmental  
17 Studies (NIES-GOSAT; Yoshida et al., 2013). Our method has three primary differences from  
18 Wunch et al. (2011b): (1) we explicitly use TCCON data from numerous sites throughout the  
19 world as reference values for the regression analysis; (2) the regression variables and  
20 coefficients for correction of GOSAT data are determined separately for observations made  
21 over land and those made over the ocean; and (3) we perform this analysis for both XCO<sub>2</sub> and  
22 XCH<sub>4</sub>. Such a partitioning is sensible because in the SWIR XCO<sub>2</sub> and XCH<sub>4</sub> retrievals, the  
23 handling of the surface reflectance is different over land and ocean. In addition, the  
24 atmosphere over ocean is generally cleaner than that over land because of the absence of  
25 polluted air and aerosols from urban areas. These differences suggest that the bias  
26 characteristics of XCO<sub>2</sub> and XCH<sub>4</sub> retrieved over ocean differ from those over land.

27

28 This paper is structured as follows. Sect. 2 presents a brief note on the datasets used and  
29 analysis procedure. In Sect. 3, we show a detailed method for correcting GOSAT data and the  
30 results of the empirical correction. Our findings and conclusions are given in Sect. 4.

31



## 1 **2 Data and analysis methods**

### 2 **2.1 XCO<sub>2</sub> and XCH<sub>4</sub> retrieved from GOSAT TANSO-FTS SWIR spectra**

3

4 To monitor the spatial distribution of atmospheric greenhouse gases from space, GOSAT was  
5 launched on 23 January 2009 into a sun-synchronous orbit with an overpass time of roughly  
6 13:00 local time (Kuze et al., 2009). Over a three-day period, TANSO-FTS onboard GOSAT  
7 makes observations above several tens of thousands of ground points spread over the earth's  
8 surface. Measurements in the SWIR and thermal infrared (TIR) bands of TANSO-FTS allow  
9 the retrievals over cloud-free regions of XCO<sub>2</sub> and XCH<sub>4</sub>, and CO<sub>2</sub> and CH<sub>4</sub> profiles,  
10 respectively. (Yoshida et al., 2011, 2013; Saitoh et al., 2012). In this study, we used Ver.  
11 02.21 XCO<sub>2</sub> and XCH<sub>4</sub> data (Yoshida et al., 2013), which cover the period from April 2009 to  
12 May 2014.

13

### 14 **2.2 TCCON data**

15 The Total Carbon Column Observing Network (TCCON) is a worldwide network of ground-  
16 based FTSS that provide time series of column-averaged abundances of various atmospheric  
17 constituents. These constituents, which include CO<sub>2</sub> and CH<sub>4</sub>, are retrieved from near-infrared  
18 solar absorption spectra using a nonlinear least-squares fitting algorithm referred to as GFIT  
19 (Wunch et al., 2010, 2011a). The TCCON data have been used to compare with satellite data  
20 and model simulations (Dils et al., 2006; Morino et al., 2011; Schneising et al., 2012; Saito et  
21 al., 2012; Heyman et al., 2012; Oshchepkov et al., 2013; Yoshida et al., 2013; Belikov et al.,  
22 2013; Dils et al., 2014; Nguyen et al., 2014; Scheepmaker et al., 2015) and elucidate the  
23 temporal behavior of greenhouse gases (Wunch et al., 2009; Deutscher et al., 2010, 2014;  
24 Messerschmidt et al., 2010; Ishizawa et al., 2015). In this study, we used TCCON data  
25 analyzed with the GGG2014 version of the standard TCCON retrieval algorithm (Wunch et  
26 al., 2015) for correction of GOSAT data. The TCCON data are available from the Carbon  
27 Dioxide Information Analysis Center (CDIAC) at <http://tcccon.ornl.gov>. The distribution and  
28 basic information of 23 TCCON sites used for correction or validation analyses of GOSAT  
29 data are shown in Fig. 1a and Table 1, respectively. The TCCON sites are distributed  
30 throughout the world including North America, Europe, Asia, and Oceania (Fig. 1a). Due to



1 the absence of coincidence with GOSAT data at Ny Ålesund, these TCCON XCO<sub>2</sub> and XCH<sub>4</sub>  
2 data were not used for correction of GOSAT data; they were, however, used for the analysis of  
3 latitudinal distributions described in Sect. 3.3.

4

### 5 **2.3 Aircraft-based data**

6 In order to test for remaining biases in the GOSAT data after applying the empirical  
7 correction developed using TCCON data, we use aircraft profile data provided by the  
8 Comprehensive Observation Network for TRace gases by AirLiner (CONTRAIL) project  
9 (Machida et al., 2008), the NOAA Earth System Research Laboratory/Global Monitoring  
10 Division (ESRL/GMD; Xiong et al., 2008; Sweeney et al., 2015), the U.S. Department of  
11 Energy (DOE; Biraud et al., 2013; Schmid et al., 2014), the National Institute for  
12 Environmental Studies (NIES; Machida et al., 2001), the Japan Meteorological Agency  
13 (JMA; Tsuboi et al., 2013), the HIAPER Pole-to-Pole Observations (HIPPO) project (Wofsy  
14 et al., 2011, 2012; Kort et al., 2012; Santoni et al., 2014), and an aircraft measurement  
15 campaign by NIES and the Japan Aerospace Exploration Agency (JAXA) (Tanaka et al.,  
16 2012). To calculate aircraft-based XCO<sub>2</sub> and XCH<sub>4</sub> (as described in the next paragraph), we  
17 also used tower data from the Meteorological Research Institute (MRI) in Tsukuba (Inoue and  
18 Matsueda, 1996, 2001) and the NOAA ESRL/GMD tall tower network in Park Falls, WI and  
19 West Branch, IA (Andrews et al., 2014). Details of the aircraft and tower measurements are  
20 described in Inoue et al. (2013) and Inoue et al. (2014), except for the JMA aircraft and  
21 ground-based measurements. The JMA aircraft measurements are conducted by utilizing the  
22 cargo aircraft C-130H of the Japan Ministry of Defense (MOD) to collect flask air samples  
23 once a month during a regular flight between the mainland of Japan and Minamitorishima, an  
24 island located nearly 2000 km southeast of Tokyo (Tsuboi et al., 2013). In addition, the JMA  
25 routinely obtains ground-based measurements at a height of 20 m over Minamitorishima. We  
26 used CO<sub>2</sub> and CH<sub>4</sub> profiles from around Minamitorishima derived from aircraft and ground-  
27 based data available via the World Data Centre for Greenhouse Gases (WDCGG) website  
28 (<http://ds.data.jma.go.jp/gmd/wdcgg/>). The typical JMA aircraft sampling altitudes were 0.5–  
29 6.5 km. Figure 1b and Table 2 show a horizontal map and basic information, respectively, on  
30 every aircraft measurement site used in this study.

31



1 Aircraft-based XCO<sub>2</sub> and XCH<sub>4</sub> are calculated by applying the GOSAT SWIR column  
2 averaging kernels (CAK) by using the methods developed by Miyamoto et al. (2013) and  
3 Inoue et al. (2014), respectively. There is one difference in the aircraft XCH<sub>4</sub> calculation:  
4 Inoue et al. (2014) used fixed monthly climatologies for the CH<sub>4</sub> profiles above the  
5 tropopause and did not include the yearly trend in CH<sub>4</sub> concentration because of their short  
6 analysis period (June 2009 to July 2010). In this study, the yearly trend is explicitly taken into  
7 account. According to recent reports from the World Meteorological Organization (WMO),  
8 global CH<sub>4</sub> abundance increased from 1789 ppb in 2007 to a high of 1824 ppb in 2013 (WMO,  
9 2008, 2014) with a growth rate of about 6 ppb yr<sup>-1</sup>. Here, we included this mean annual trend  
10 (6 ppb yr<sup>-1</sup>) of CH<sub>4</sub> profiles above the tropopause for the calculation of aircraft-based XCH<sub>4</sub>.

11

## 12 **2.4 Correction and validation procedure of GOSAT data**

13 Our aim in this study is to correct GOSAT SWIR XCO<sub>2</sub> and XCH<sub>4</sub> (Ver. 02.21) by multiple  
14 linear regression using TCCON data as reference values. In Sect. 3.1, we explain the details  
15 of the empirical correction method. To evaluate the effectiveness of this correction method,  
16 we compare uncorrected/corrected GOSAT XCO<sub>2</sub> (XCH<sub>4</sub>) to independent aircraft-based  
17 XCO<sub>2</sub> (XCH<sub>4</sub>) based on aircraft measurements by CONTRAIL, NOAA, DOE, NIES, JMA,  
18 the HIPPO project, and the NIES-JAXA joint campaign (Sect. 3.2). We compare GOSAT  
19 data retrieved on the same day and within ±5° latitude/longitude boxes centered on each  
20 aircraft profile. We also investigate the spatial distributions of uncorrected/corrected GOSAT  
21 data (Sect. 3.3), and the temporal behavior of the GOSAT XCO<sub>2</sub> and XCH<sub>4</sub> biases (Sect. 3.4).

22

## 23 **3 Results and discussion**

### 24 **3.1 Parameter dependency of GOSAT biases and multiple linear regression** 25 **for correction of GOSAT data**

26 The bias correction of GOSAT XCO<sub>2</sub> and XCH<sub>4</sub> (Ver. 02.21) uses multiple linear regression.  
27 Before formulating the regression equations, we perform a correlation analysis between the  
28 GOSAT biases and simultaneously-retrieved auxiliary parameters at TCCON sites. Here, the  
29 differences between GOSAT XCO<sub>2</sub> (XCH<sub>4</sub>) and TCCON XCO<sub>2</sub> (XCH<sub>4</sub>) are referred to as  
30 ΔXCO<sub>2</sub> (ΔXCH<sub>4</sub>). Figures 2a–d and 3a show several examples of scatter diagrams between



1  $\Delta XCO_2$  (or  $\Delta XCH_4$ ) and simultaneously-retrieved auxiliary parameters obtained within  $\pm 5^\circ$   
 2 latitude/longitude boxes centered at respective TCCON sites. The GOSAT data retrieved over  
 3 land and ocean regions are described by green and blue dots, respectively. For instance,  
 4  $\Delta XCO_2$  has a significant negative correlation with the difference between the retrieved  
 5 surface pressure and a priori surface pressure ( $\Delta P_s$ ; Fig. 2b), which suggests that error in the  
 6 surface pressure retrieval ( $\Delta P_s$ ) is, in part, responsible for the presence of the GOSAT  $XCO_2$   
 7 biases. Thus, we examined the correlations between the GOSAT biases and more than 20  
 8 other parameters retrieved from GOSAT TANSO-FTS, and investigated which combinations  
 9 of available parameters led to a reduction of the GOSAT biases due to the linear regression.  
 10 For the correction of  $XCO_2$  retrievals, we selected four parameters to include in bias  
 11 corrections; the retrieved aerosol optical depth (AOD),  $\Delta P_s$ , airmass, and surface albedo for  
 12 the  $O_2$  A-band. The derived bias correction for  $XCO_2$  is

$$13 \quad X_{CO_2}^{modified} = X_{CO_2}^{retrieved} + C_0 - C_1(AOD - \overline{AOD}) - C_2(\Delta P_s - \overline{\Delta P_s}) \\ - C_3(airmass - \overline{airmass}) - C_4(albedo_{O_2} - \overline{albedo_{O_2}}). \quad (1)$$

14 However, only the retrieved AOD was selected for  $XCH_4$  retrievals. The bias correction for  
 15  $XCH_4$  is

$$16 \quad X_{CH_4}^{modified} = X_{CH_4}^{retrieved} + C_0 - C_1(AOD - \overline{AOD}). \quad (2)$$

17 Here,  $X_{CO_2}^{retrieved}$  and  $X_{CH_4}^{retrieved}$  are the GOSAT  $XCO_2$  and  $XCH_4$  retrievals, respectively (i.e.,  
 18 uncorrected GOSAT data).  $X_{CO_2}^{modified}$  and  $X_{CH_4}^{modified}$  denote the corrected GOSAT  $XCO_2$  and  
 19  $XCH_4$  data, respectively. AOD represents the retrieved aerosol optical depth, and  $\Delta P_s$  is the  
 20 difference between the retrieved surface pressure and the a priori surface pressure. Airmass is  
 21 a simple function of the solar zenith angle  $\theta_z$  and the satellite-viewing angle  $\theta_v$  and can be  
 22 approximated as

$$23 \quad airmass = \frac{1}{\cos \theta_z} + \frac{1}{\cos \theta_v}. \quad (3)$$

24 In addition,  $albedo_{O_2}$  is the surface albedo for the  $O_2$  A-band, which is retrieved only for  
 25 land. The overbars denote averages of all GOSAT data used for the regression analysis.  $C_0$  is  
 26 the regression coefficient for the bias, and  $C_1$ ,  $C_2$ ,  $C_3$ , and  $C_4$  are the regression coefficients  
 27 for the respective parameters, that are used for the correction of GOSAT data. As described in





1 the next paragraph, we determined these regression coefficients separately for land and ocean  
2 regions.  
3  
4 Table 3 shows the regression coefficients obtained via the multiple linear regression analyses.  
5 The coefficients,  $C_0$ – $C_4$ , were determined as follows: To prepare the TCCON  $XCO_2$  and  
6  $XCH_4$  as reference values for the multiple regression analysis, we made a connection between  
7 the GOSAT data retrieved within  $\pm 5^\circ$  latitude/longitude boxes centered at respective TCCON  
8 sites and mean values of TCCON data (GGG2014 version) observed within  $\pm 30$  min of the  
9 GOSAT overpass time. Averages and the standard deviations (SD) of the differences between  
10 uncorrected GOSAT data and TCCON data at each site are listed in Table 4 for  $XCO_2$  and  
11 Table 5 for  $XCH_4$ . Figures 4a and 4c are scatter diagrams between uncorrected GOSAT data  
12 and TCCON data at all TCCON sites for  $XCO_2$  and  $XCH_4$ , respectively. For  $XCO_2$ , we  
13 identify 8245 samples for land and 544 samples for ocean that satisfy the coincident criteria.  
14 We find that global mean biases of GOSAT  $XCO_2$  retrievals (i.e., uncorrected GOSAT  
15  $XCO_2$ ) over land and ocean regions against the TCCON data were  $-0.86$  ppm (SD = 2.18  
16 ppm) and  $-1.90$  ppm (SD = 1.72 ppm), respectively (Table 4). The average and standard  
17 deviation of the GOSAT biases derived from respective TCCON sites (hereafter referred to as  
18 station bias) over land are  $-0.43$  ppm and  $0.87$  ppm, respectively. Correlation coefficients  
19 between two  $XCO_2$  datasets were 0.89 over land and 0.90 over ocean (Fig. 4a). The mean  
20 biases of uncorrected GOSAT  $XCH_4$  over land and ocean regions were  $-6.0$  ppb (SD = 15.2  
21 ppb) and  $-0.2$  ppb (SD = 13.4 ppb), respectively (Table 5). Correlation coefficients between  
22 both  $XCH_4$  datasets were 0.85 over land and 0.91 over ocean (Fig. 4c). The results over land  
23 are similar to those of Yoshida et al. (2013) who validated GOSAT  $XCO_2$  and  $XCH_4$  data  
24 (Ver. 02.xx), although the versions of the TCCON data used in their study (the previous  
25 GGG2012 version) and our present study differ. Conducting the regression analysis using Eqs.  
26 (1) and (2), the regression coefficients for correction of GOSAT  $XCO_2$  (and  $XCH_4$ ) were  
27 determined separately for land and ocean regions (Table 3). Because surface albedo is not  
28 retrieved over ocean, the terms including  $C_4$  in Eq. (1) were neglected for determining the  
29 regression coefficients for  $XCO_2$  over ocean. The GOSAT data were obtained through two  
30 different TANSO-FTS modes: medium gain (Gain-M) utilized over bright land surfaces  
31 including the Sahara Desert and high gain (Gain-H) used elsewhere (Yoshida et al., 2013).  
32 Note that the regression coefficients are calculated from GOSAT data retrieved within  $\pm 5^\circ$



1 boxes centered at 20 TCCON sites, that are located in Gain-H regions even though we aim to  
2 correct GOSAT XCO<sub>2</sub> and XCH<sub>4</sub> data from around the world, including Gain-H and Gain-M  
3 regions. Additionally, we take the mean difference between TCCON XCH<sub>4</sub> and aircraft-based  
4 XCH<sub>4</sub> into account when calculating the coefficients C<sub>0</sub> over land and ocean for XCH<sub>4</sub>. In a  
5 comparative analysis at four locations, Inoue et al. (2014) showed that aircraft-based XCH<sub>4</sub>  
6 was 8.6 ppb smaller than TCCON XCH<sub>4</sub> on average. Consequently, in this study, we used the  
7 values for C<sub>0</sub> shown in Table 3b (i.e., 6.0 ppb over land and 0.2 ppb over ocean) for the  
8 correction of GOSAT XCH<sub>4</sub> when comparing GOSAT XCH<sub>4</sub> with TCCON XCH<sub>4</sub>. In contrast,  
9 the values for C<sub>0</sub> shown in Table 3b with 8.6 ppb subtracted (i.e., -2.6 ppb over land and -8.4  
10 ppb over ocean) were used when comparing the GOSAT XCH<sub>4</sub> with the aircraft-based XCH<sub>4</sub>.  
11 Figures 2e–h and 3b are scatter diagrams between the biases of GOSAT data ( $\Delta$ XCO<sub>2</sub> and  
12  $\Delta$ XCH<sub>4</sub>) corrected by these regression coefficients C<sub>0</sub>–C<sub>4</sub> (Table 3) and simultaneously  
13 retrieved parameters. After correction, the correlation coefficients between  $\Delta$ XCO<sub>2</sub> (or  
14  $\Delta$ XCH<sub>4</sub>) and respective parameters were approximately zero.

15

16 We compare the GOSAT XCO<sub>2</sub> and XCH<sub>4</sub> corrected using the regression coefficients to the  
17 TCCON XCO<sub>2</sub> and XCH<sub>4</sub> (Tables 4–5, and Figs. 4b and 4d). Using this empirical correction,  
18 the global mean biases of GOSAT XCO<sub>2</sub> relative to the TCCON data became zero over both  
19 land (change from -0.86 ppm to 0.00 ppm) and ocean (-1.90 ppm to -0.01 ppm). Correlation  
20 coefficients between GOSAT XCO<sub>2</sub> and TCCON XCO<sub>2</sub> became somewhat higher over land  
21 (0.89 to 0.91). Table 5 shows that the mean biases of GOSAT XCH<sub>4</sub> also became zero over  
22 both land (-6.0 ppb to 0.0 ppb) and ocean (-0.2 ppb to -0.1 ppb). Clearly, as expected, the  
23 GOSAT XCO<sub>2</sub> and XCH<sub>4</sub> biases were reduced after correction. This, of course, is a natural  
24 consequence because the GOSAT data approached the TCCON values after applying the  
25 corrections. Therefore, in the next section, we validate the GOSAT XCO<sub>2</sub> and XCH<sub>4</sub>  
26 corrected by TCCON data using independent aircraft measurement data instead of TCCON  
27 data.

28



## 1 **3.2 Comparisons between uncorrected/corrected GOSAT data and aircraft-** 2 **based data**

3 To confirm the effectiveness of the empirical correction, we compare uncorrected/corrected  
4 GOSAT data with aircraft-based data. Figure 5 shows scatter diagrams between  
5 uncorrected/corrected GOSAT data and aircraft-based data at all aircraft observation sites.  
6 Tables 6 and 7 indicate the differences between uncorrected/corrected GOSAT data and  
7 aircraft-based data for XCO<sub>2</sub> and XCH<sub>4</sub> at each aircraft site, respectively. The average  
8 differences between uncorrected GOSAT XCO<sub>2</sub> and aircraft-based XCO<sub>2</sub> over land and ocean  
9 within ±5° latitude/longitude boxes were -0.85 ppm (SD = 2.48 ppm) and -2.08 ppm (SD =  
10 1.69 ppm), respectively (Table 6). The correction reduced the mean biases of GOSAT XCO<sub>2</sub>  
11 to below twentieth over land (-0.85 ppm to -0.04 ppm) and to below one-sixth over ocean (-  
12 2.08 ppm to -0.32 ppm). The averages of the XCO<sub>2</sub> station bias over land and ocean are also  
13 smaller after correction. The correlation coefficients between GOSAT XCO<sub>2</sub> and aircraft-  
14 based XCO<sub>2</sub> over land became higher after correction (0.86 to 0.88). For XCH<sub>4</sub>, the average  
15 differences between uncorrected GOSAT XCH<sub>4</sub> and aircraft-based XCH<sub>4</sub> over land and ocean  
16 were 4.5 ppb (SD = 15.2 ppb) and 6.6 ppb (SD = 12.8 ppb), respectively (Table 7). The global  
17 mean biases of GOSAT XCH<sub>4</sub> relative to aircraft measurements were also reduced by half  
18 over land (4.5 ppb to 2.2 ppb) and reduced to about one-quarter over ocean (6.6 ppb to -1.7  
19 ppb). The correlation coefficients between GOSAT XCH<sub>4</sub> and aircraft-based XCH<sub>4</sub> over land  
20 became higher (0.70 to 0.71). Thus, the bias correction improves the accuracy and precision  
21 of the GOSAT data for both XCO<sub>2</sub> and XCH<sub>4</sub>.

22

## 23 **3.3 Spatial distributions of uncorrected/corrected GOSAT data**

24 We next applied the regression coefficients C<sub>0</sub>–C<sub>4</sub> calculated from samples around only 20  
25 TCCON sites to all GOSAT XCO<sub>2</sub> and XCH<sub>4</sub> data around the world, and we examined how  
26 the global distributions of GOSAT data changed due to this empirical correction. Figures 6a  
27 and 6b indicate the horizontal distributions of uncorrected GOSAT XCO<sub>2</sub> and corrected  
28 GOSAT XCO<sub>2</sub>, respectively, in July 2009. In the Northern summer, the CO<sub>2</sub> concentration  
29 over Siberia is significantly lower due to forest absorption of CO<sub>2</sub> through photosynthesis  
30 (e.g., Nakazawa et al., 1997; Guerlet et al., 2013). The differences between corrected GOSAT  
31 XCO<sub>2</sub> and uncorrected GOSAT XCO<sub>2</sub> are shown in Fig. 6c. As noted above, GOSAT XCO<sub>2</sub>



1 has a negative bias of about 1–2 ppm over land and ocean regions. Therefore, the bias  
2 correction increases XCO<sub>2</sub> in most parts of the world (Fig. 6c). In the middle of South  
3 America and southern Africa, however, GOSAT XCO<sub>2</sub> became smaller after correction. We  
4 next focus on the horizontal distributions of uncorrected/corrected GOSAT XCH<sub>4</sub> in July  
5 2009 (Figs. 6d and 6e). Figure 6d shows that CH<sub>4</sub> concentrations in the Northern Hemisphere  
6 are higher than those in the Southern Hemisphere. In particular, there are distinct features of  
7 high CH<sub>4</sub> concentrations around the eastern United States, the Middle East, western Siberia,  
8 and East Asia in the Northern Hemisphere and low CH<sub>4</sub> concentrations over southern South  
9 America, southern Africa, and Australia, with a larger gradient in the Southern Hemisphere.  
10 After correction, GOSAT XCH<sub>4</sub> became 4–8 ppb higher over most land regions (Fig. 6f),  
11 consistent with comparisons to the TCCON data over land (Sect. 3.1). XCH<sub>4</sub> over the ocean  
12 became smaller at low latitudes in the Northern Hemisphere (0°–20°N) such as the Atlantic  
13 Ocean, and became larger in mid-latitudes (20°–40°N).

14

15 It is difficult to evaluate whether the GOSAT data across the globe are improved by using the  
16 regression coefficients C<sub>0</sub>–C<sub>4</sub> derived exclusively from around TCCON sites, due to the  
17 sparseness of the ground-based and aircraft measurements in many regions around the world.  
18 Accordingly, we investigated the latitudinal distributions of the uncorrected/corrected  
19 GOSAT data, the TCCON data, and the aircraft-based data, and then compared the three  
20 datasets for July 2009 (Fig. 7). We prepared zonal-mean monthly averages of the GOSAT  
21 data retrieved in each 15° latitudinal band. For example, averages of GOSAT XCO<sub>2</sub> obtained  
22 over land and ocean regions within a latitudinal band from the equator to 15°N in July 2009  
23 are represented by black and green dots, respectively, around 7.5°N in Fig. 7a. The TCCON  
24 data are mean values measured within ±30 min of the GOSAT overpass time (e.g., about  
25 12:50 pm local time in Tsukuba) on all days when TCCON data were obtained in July 2009.  
26 Aircraft-based data are monthly averages of all data obtained at each aircraft observation site.  
27 In July 2009, GOSAT XCO<sub>2</sub> data were underestimated by about 1–2 ppm compared to the  
28 reference data (Fig. 7a). We found that corrected GOSAT XCO<sub>2</sub> was consistent with the  
29 TCCON XCO<sub>2</sub> and aircraft-based XCO<sub>2</sub> in both hemispheres, though the variability of  
30 aircraft-based XCO<sub>2</sub> was relatively large in mid-latitudes (Fig. 7b). Figure 7c shows  
31 latitudinal distributions of uncorrected GOSAT XCH<sub>4</sub>, TCCON XCH<sub>4</sub>, and aircraft-based  
32 XCH<sub>4</sub>. XCH<sub>4</sub> in the Northern Hemisphere is higher than that in the Southern Hemisphere in



1 July (Fig. 7c), because the main CH<sub>4</sub> sources are terrestrial, including rice paddy fields and  
2 wetlands. In addition, the latitudinal variation in XCH<sub>4</sub> shows a larger meridional gradient in  
3 the Southern Hemisphere (Fig. 7c), which is consistent with the global distribution of XCH<sub>4</sub>  
4 (Fig. 6d). The uncorrected GOSAT XCH<sub>4</sub> was negatively biased against the TCCON data.  
5 The empirical correction resulted in a marked decrease in GOSAT XCH<sub>4</sub> biases on the same  
6 latitudinal bands as several TCCON sites (e.g., Ny Ålesund, Sodankylä, and Lauder) over both  
7 hemispheres (Fig. 7d). Thus, the correction method is very effective for reducing the biases of  
8 the GOSAT XCO<sub>2</sub> and XCH<sub>4</sub>, from the standpoint of the spatial distributions.

9

#### 10 **3.4 Temporal behaviors of uncorrected/corrected GOSAT data and the** 11 **GOSAT biases**

12 Finally, we investigated temporal variations in GOSAT XCO<sub>2</sub> and XCH<sub>4</sub> data and the  
13 GOSAT biases. We focused on the 30°–45°N latitudinal band, which includes the Lamont site  
14 where most monthly data were available during the analysis period. Figure 8a shows the  
15 temporal variations of uncorrected GOSAT XCO<sub>2</sub>, TCCON XCO<sub>2</sub> at Tsukuba and Lamont,  
16 and aircraft-based XCO<sub>2</sub> at Narita. Along with the example of July 2009 in Sect. 3.3, zonal-  
17 mean GOSAT XCO<sub>2</sub> retrieved over land and ocean regions within a 30°–45°N latitudinal  
18 band, TCCON XCO<sub>2</sub> and aircraft-based XCO<sub>2</sub> at several sites included in a 30°–45°N  
19 latitudinal band were calculated for all months during the analysis period. The temporal  
20 variations in the three datasets revealed that XCO<sub>2</sub> is higher in Northern spring (April and  
21 May) and lower in August and September (Fig. 8a). XCO<sub>2</sub> has a seasonal amplitude of  
22 approximately 7–12 ppm at mid-latitudes over the Northern Hemisphere. In this study, the  
23 growth rate of uncorrected GOSAT XCO<sub>2</sub> was roughly 2.5 ppm yr<sup>-1</sup> from 2009 to 2013,  
24 while Inoue et al. (2013) showed that the growth rate of aircraft-based XCO<sub>2</sub> at most sites was  
25 about 2.0 ppm yr<sup>-1</sup> from 2007 to 2010. This is consistent with the rapid increase of CO<sub>2</sub>  
26 emissions over the last few years. After bias correction, the temporal variability in the  
27 GOSAT XCO<sub>2</sub> agrees well with those of the TCCON and aircraft measurements (Fig. 8b).  
28 Moreover, the uncorrected GOSAT XCO<sub>2</sub> data were negatively biased (Fig. 8c), however,  
29 this time series has a seasonality wherein the negative biases of GOSAT XCO<sub>2</sub> become higher  
30 around July and August. After bias correction, the XCO<sub>2</sub> biases for many months approach  
31 zero, though the seasonality in the difference remains (Fig. 8d).



1

2 Figure 9a shows the temporal behavior of zonal-mean uncorrected GOSAT XCH<sub>4</sub> and XCH<sub>4</sub>  
3 at the Tsukuba and Lamont TCCON sites. GOSAT XCH<sub>4</sub> is higher in September and October,  
4 and lower in February and March than the reference data. Although the GOSAT XCH<sub>4</sub> data  
5 retrieved over land were negatively biased except for summer during the analysis period (Figs.  
6 9a and 9c), the GOSAT XCH<sub>4</sub> biases were reduced as a result of the empirical correction  
7 (Figs. 9b and 9d). Consequently, we suggest that the bias correction method was effective for  
8 GOSAT XCO<sub>2</sub> and XCH<sub>4</sub>.

9

#### 10 **4 Summary and conclusions**

11 In this study, we correct XCO<sub>2</sub> and XCH<sub>4</sub> data (Ver. 02.21) retrieved from the GOSAT  
12 TANSO-FTS SWIR spectra. First, we conducted correlation analyses between the GOSAT  
13 biases and the simultaneously-retrieved auxiliary parameters, using GOSAT data around  
14 TCCON sites. Based on the results, we selected several parameters and determined the  
15 regression coefficients for the correction of GOSAT XCO<sub>2</sub> and XCH<sub>4</sub> for land and ocean  
16 regions separately. To evaluate the effectiveness of the bias correction method, the  
17 uncorrected/corrected GOSAT XCO<sub>2</sub> and XCH<sub>4</sub> data were compared to aircraft  
18 measurements provided by CONTRAIL, NOAA, DOE, NIES, JMA, the HIPPO project, and  
19 the NIES-JAXA joint campaign. After correction, biases of GOSAT XCO<sub>2</sub> were reduced by a  
20 factor of more than 20 over land and by a factor of six over ocean, while the biases of  
21 GOSAT XCH<sub>4</sub> were reduced by half over land and became by almost a quarter of their  
22 uncorrected values over ocean. We thus demonstrated that our empirical method using  
23 multiple linear regression is useful for the bias correction of GOSAT XCO<sub>2</sub> and XCH<sub>4</sub>.

24

#### 25 **Acknowledgments**

26 The authors thank the many staff members of Japan Airlines, the JAL Foundation, and  
27 JAMCO Tokyo for supporting the CONTRAIL project. We are grateful to the NOAA  
28 ESRL/GMD tall tower network (K. Davis, A. Desai, R. Teclaw, D. Baumann, and C. Stanier)  
29 for providing CO<sub>2</sub> tower data for Park Falls and West Branch. DOE flights were supported by  
30 the Office of Biological and Environmental Research of the U.S. Department of Energy under  
31 contract No. DE-AC02-05CH11231 as part of the Atmospheric Radiation Measurement



1 Program (ARM), ARM Aerial Facility, and Terrestrial Ecosystem Science Program. We  
2 gratefully thank many staff members of the Japan Ministry of Defense for supporting the  
3 JMA's ground-based and aircraft measurements. We also acknowledge the HIPPO team  
4 members for CO<sub>2</sub> and CH<sub>4</sub> profile data from HIPPO missions. The HIPPO program is  
5 supported by the National Science Foundation (NSF), and its operation is managed by the  
6 Earth Observing Laboratory (EOL) of the National Center for Atmospheric Research (NCAR).  
7 We also thank the Canadian Space Agency (CSA), which provides most of the funding  
8 support for ACE. We are grateful to the HALOE team for publishing their data for scientific  
9 use. This research was supported in part by the Environment Research and Technology  
10 Development Fund (2A-1102) of the Ministry of the Environment, Japan. TCCON  
11 measurements from Pasadena, Lamont, Park Falls and Darwin are funded by NASA grant  
12 NNX14AI60G and NASA Orbiting Carbon Observatory Program. We are grateful to the  
13 DOE ARM program for technical support of TCCON in Lamont and Darwin and to Jeff  
14 Ayers for technical support of the TCCON measurements in Park Falls. Darwin and  
15 Wollongong TCCON measurements are also supported by Australian Research Council grant  
16 DP140101552 and Nicholas Deutscher is supported by an ARC-DECRA Fellowship,  
17 DE140100178. The University of Bremen acknowledges the support of the EU projects  
18 InGOS, and ICOS-INWIRE, and the Senate of Bremen for support of TCCON measurements  
19 in Białystok, Bremen, Ny Ålesund, and Orléans. Operation of the Ascension Island site was  
20 funded by the Max Planck Society. Research at the FMI was supported by the Academy of  
21 Finland under grant number 140408.

22

## 23 **References**

24 Andrews, A. E., Kofler, J. D., Trudeau, M. E., Williams, J. C., Neff, D. H., Masarie, K. A.,  
25 Chao, D. Y., Kitzis, D. R., Novelli, P. C., Zhao, C. L., Dlugokencky, E. J., Lang, P. M.,  
26 Crotwell, M. J., Fischer, M. L., Parker, M. J., Lee, J. T., Baumann, D. D., Desai, A. R.,  
27 Stanier, C. O., De Wekker, S. F. J., Wolfe, D. E., Munger, J. W., and Tans, P. P.: CO<sub>2</sub>, CO,  
28 and CH<sub>4</sub> measurements from tall towers in the NOAA Earth System Research Laboratory's  
29 Global Greenhouse Gas Reference Network: instrumentation, uncertainty analysis, and  
30 recommendations for future high-accuracy greenhouse gas monitoring efforts, Atmos. Meas.  
31 Tech., 7, 647-687, doi:10.5194/amt-7-647-2014, 2014.

32



- 1 Belikov, D. A., Maksyutov, S., Sherlock, V., Aoki, S., Deutscher, N. M., Dohe, S., Griffith,  
2 D., Kyro, E., Morino, I., Nakazawa, T., Notholt, J., Rettinger, M., Schneider, M., Sussmann,  
3 R., Toon, G. C., Wennberg, P. O., and Wunch, D.: Simulations of column-averaged CO<sub>2</sub> and  
4 CH<sub>4</sub> using the NIES TM with a hybrid sigma-isentropic ( $\sigma$ - $\theta$ ) vertical coordinate, Atmos.  
5 Chem. Phys., 13, 1713-1732, doi:10.5194/acp-13-1713-2013, 2013.
- 6
- 7 Biraud, S. C., Torn, M. S., Smith, J. R., Sweeney, C., Riley, W. J., and Tans, P. P.: A multi-  
8 year record of airborne CO<sub>2</sub> observations in the US Southern Great Plains, Atmos. Meas.  
9 Tech., 6, 751-763, doi:10.5194/amt-6-751-2013, 2013.
- 10
- 11 Crisp, D., Fisher, B. M., O'Dell, C., Frankenberg, C., Basilio, R., Bösch, H., Brown, L. R.,  
12 Castano, R., Connor, B., Deutscher, N. M., Eldering, A., Griffith, D., Gunson, M., Kuze, A.,  
13 Mandrake, L., McDuffie, J., Messerschmidt, J., Miller, C. E., Morino, I., Natraj, V., Notholt,  
14 J., O'Brien, D. M., Oyafuso, F., Polonsky, I., Robinson, J., Salawitch, R., Sherlock, V., Smyth,  
15 M., Suto, H., Taylor, T. E., Thompson, D. R., Wennberg, P. O., Wunch, D., and Yung, Y. L.:  
16 The ACOS CO<sub>2</sub> retrieval algorithm – Part II: Global XCO<sub>2</sub> data characterization, Atmos.  
17 Meas. Tech., 5, 687-707, doi:10.5194/amt-5-687-2012, 2012.
- 18
- 19 Deng, F., Jones, D. B. A., Henze, D. K., Bousserez, N., Bowman, K. W., Fisher, J. B., Nassar,  
20 R., O'Dell, C., Wunch, D., Wennberg, P. O., Kort, E. A., Wofsy, S. C., Blumenstock, T.,  
21 Deutscher, N. M., Griffith, D. W. T., Hase, F., Heikkinen, P., Sherlock, V., Strong, K.,  
22 Sussmann, R., and Warneke, T.: Inferring regional sources and sinks of atmospheric CO<sub>2</sub>  
23 from GOSAT XCO<sub>2</sub> data, Atmos. Chem. Phys., 14, 3703-3727, doi:10.5194/acp-14-3703-  
24 2014, 2014.
- 25
- 26 Deutscher, N. M., Griffith, D. W. T., Bryant, G. W., Wennberg, P. O., Toon, G. C.,  
27 Washenfelder, R. A., Keppel-Aleks, G., Wunch, D., Yavin, Y., Allen, N. T., Blavier, J.-F.,  
28 Jiménez, R., Daube, B. C., Bright, A. V., Matross, D. M., Wofsy, S. C., and Park, S.: Total  
29 column CO<sub>2</sub> measurements at Darwin, Australia – site description and calibration against in  
30 situ aircraft profiles, Atmos. Meas. Tech., 3, 947-958, doi:10.5194/amt-3-947-2010, 2010.





1

2 Deutscher, N. M., Sherlock, V., Mikaloff Fletcher, S. E., Griffith, D. W. T., Notholt, J.,  
3 Macatangay, R., Connor, B. J., Robinson, J., Shiona, H., Velazco, V. A., Wang, Y.,  
4 Wennberg, P. O., and Wunch, D.: Drivers of column-average CO<sub>2</sub> variability at Southern  
5 Hemispheric Total Carbon Column Observing Network sites, *Atmos. Chem. Phys.*, 14, 9883-  
6 9901, doi:10.5194/acp-14-9883-2014, 2014.

7

8 Dils, B., De Mazière, M., Müller, J. F., Blumenstock, T., Buchwitz, M., de Beek, R.,  
9 Demoulin, P., Duchatelet, P., Fast, H., Frankenberg, C., Gloudemans, A., Griffith, D., Jones,  
10 N., Kerzenmacher, T., Kramer, I., Mahieu, E., Mellqvist, J., Mittermeier, R. L., Notholt, J.,  
11 Rinsland, C. P., Schrijver, H., Smale, D., Strandberg, A., Straume, A. G., Stremme, W.,  
12 Strong, K., Sussmann, R., Taylor, J., van den Broek, M., Velazco, V., Wagner, T., Warneke,  
13 T., Wiacek, A., and Wood, S.: Comparisons between SCIAMACHY and ground-based FTIR  
14 data for total columns of CO, CH<sub>4</sub>, CO<sub>2</sub> and N<sub>2</sub>O, *Atmos. Chem. Phys.*, 6, 1953-1976,  
15 doi:10.5194/acp-6-1953-2006, 2006.

16

17 Dils, B., Buchwitz, M., Reuter, M., Schneising, O., Boesch, H., Parker, R., Guerlet, S., Aben,  
18 I., Blumenstock, T., Burrows, J. P., Butz, A., Deutscher, N. M., Frankenberg, C., Hase, F.,  
19 Hasekamp, O. P., Heymann, J., De Mazière, M., Notholt, J., Sussmann, R., Warneke, T.,  
20 Griffith, D., Sherlock, V., and Wunch, D.: The Greenhouse Gas Climate Change Initiative  
21 (GHG-CCI): comparative validation of GHG-CCI SCIAMACHY/ENVISAT and TANSO-  
22 FTS/GOSAT CO<sub>2</sub> and CH<sub>4</sub> retrieval algorithm products with measurements from the TCCON,  
23 *Atmos. Meas. Tech.*, 7, 1723-1744, doi:10.5194/amt-7-1723-2014, 2014.

24

25 Gavrilov, N. M., Makarova, M. V., Poberovskii, A. V., and Timofeyev, Yu. M.: Comparisons  
26 of CH<sub>4</sub> ground-based FTIR measurements near Saint Petersburg with GOSAT observations,  
27 *Atmos. Meas. Tech.*, 7, 1003-1010, doi:10.5194/amt-7-1003-2014, 2014.

28



- 1 Guerlet, S., Basu, S., Butz, A., Krol, M., Hahne, P., Houweling, S., Hasekamp, O. P., and  
2 Aben, I.: Reduced carbon uptake during the 2010 Northern Hemisphere summer from  
3 GOSAT, *Geophys. Res. Lett.*, **40**, 2378-2383, doi:10.1002/grl.50402, 2013.
- 4
- 5 Heymann, J., Bovensmann, H., Buchwitz, M., Burrows, J. P., Deutscher, N. M., Notholt, J.,  
6 Rettinger, M., Reuter, M., Schneising, O., Sussmann, R., and Warneke, T.: SCIAMACHY  
7 WFM-DOAS XCO<sub>2</sub>: reduction of scattering related errors, *Atmos. Meas. Tech.*, **5**, 2375-2390,  
8 doi:10.5194/amt-5-2375-2012, 2012.
- 9
- 10 Inoue, H. Y. and Matsueda, H.: Variations in atmospheric CO<sub>2</sub> at the Meteorological  
11 Research Institute, Tsukuba, Japan, *J. Atmos. Chem.*, **23**, 137-161, 1996.
- 12
- 13 Inoue, H. Y. and Matsueda, H.: Measurements of atmospheric CO<sub>2</sub> from a meteorological  
14 tower in Tsukuba, Japan, *Tellus B*, **53**, 205-219, doi:10.1034/j.1600-0889.2001.01163.x, 2001.
- 15
- 16 Inoue, M., Morino, I., Uchino, O., Miyamoto, Y., Yoshida, Y., Yokota, T., Machida, T., Sawa,  
17 Y., Matsueda, H., Sweeney, C., Tans, P. P., Andrews, A. E., Biraud, S. C., Tanaka, T.,  
18 Kawakami, S., and Patra, P. K.: Validation of XCO<sub>2</sub> derived from SWIR spectra of GOSAT  
19 TANSO-FTS with aircraft measurement data, *Atmos. Chem. Phys.*, **13**, 9771-9788,  
20 doi:10.5194/acp-13-9771-2013, 2013.
- 21
- 22 Inoue, M., Morino, I., Uchino, O., Miyamoto, Y., Saeki, T., Yoshida, Y., Yokota, T.,  
23 Sweeney, C., Tans, P. P., Biraud, S. C., Machida, T., Pittman, J. V., Kort, E. A., Tanaka, T.,  
24 Kawakami, S., Sawa, Y., Tsuboi, K., and Matsueda, H.: Validation of XCH<sub>4</sub> derived from  
25 SWIR spectra of GOSAT TANSO-FTS with aircraft measurement data, *Atmos. Meas. Tech.*,  
26 **7**, 2987-3005, doi:10.5194/amt-7-2987-2014, 2014.
- 27
- 28 Ishizawa, M., Shirai, T., Inoue, M., Morino, I., Yoshida, Y., Zhuravlev, R., Ganshin, A.,  
29 Belikov, D., Saito, M., Oda, T., Valsala, V., Uchino, O., Yokota, T., and Maksyutov, S.:



- 1 Impact of retrieval biases of GOSAT XCO<sub>2</sub> on the surface CO<sub>2</sub> flux estimates, Soon to be  
2 submitted to J. Geophys. Res.
- 3
- 4 Ishizawa, M., Uchino, O., Morino, I., Inoue, M., Yoshida, Y., Mabuchi, K., Shirai, T.,  
5 Tohjima, Y., Maksyutov, S., Ohya, H., Kawakami, S., and Takizawa, A.: Large XCH<sub>4</sub>  
6 anomaly in summer 2013 over Northeast Asia observed by GOSAT, Atmos. Chem. Phys.  
7 Discuss., 15, 24995-25020, doi:10.5194/acpd-15-24995-2015, 2015.
- 8
- 9 Kort, E. A., Wofsy, S. C., Daube, B. C., Diao, M., Elkins, J. W., Gao, R. S., Hints, E. J.,  
10 Hurst, D. F., Jimenez, R., Moore, F. L., Spackman, J. R., and Zondlo, M. A.: Atmospheric  
11 observations of Arctic Ocean methane emissions up to 82° north, Nature Geoscience, 5, 318-  
12 321, doi:10.1038/ngeo1452, 2012.
- 13
- 14 Kuze, A., Suto, H., Nakajima, M., and Hamazaki, T.: Thermal and near infrared sensor for  
15 carbon observation Fourier-transform spectrometer on the Greenhouse Gases Observing  
16 Satellite for greenhouse gases monitoring, Applied Optics, 48, 6716-6733  
17 doi:10.1364/AO.48.006716, 2009.
- 18
- 19 Machida, T., Nakazawa, T., Ishido, S., Maksyutov, S., Tohjima, Y., Takahashi, Y., Watai,  
20 T., Vinnichenko, N., Panchenko, M., Arshinov, M., Fedoseev, N., and Inoue, G: Temporal  
21 and spatial variations of atmospheric CO<sub>2</sub> mixing ratio over Siberia, Ext. Abstr. 6th  
22 International CO<sub>2</sub> Conf., 1-5 October, Sendai, Japan, 2001.
- 23
- 24 Machida, T., Matsueda, H., Sawa, Y., Nakagawa, Y., Hirokuni, K., Kondo, N., Goto, K.,  
25 Nakazawa, T., Ishikawa, K., and Ogawa, T.: Worldwide measurements of atmospheric CO<sub>2</sub>  
26 and other trace gas species using commercial airlines, J. Atmos. Oceanic. Technol., 25, 1744-  
27 1754, doi:10.1175/2008JTECHA1082.1, 2008.
- 28



- 1 Maksyutov, S., Takagi, H., Valsala, V. K., Saito, M., Oda, T., Saeki, T., Belikov, D. A., Saito,  
2 R., Ito, A., Yoshida, Y., Morino, I., Uchino, O., Andres, R. J., and Yokota, T.: Regional CO<sub>2</sub>  
3 flux estimates for 2009–2010 based on GOSAT and ground-based CO<sub>2</sub> observations, Atmos.  
4 Chem. Phys., 13, 9351-9373, doi:10.5194/acp-13-9351-2013, 2013.
- 5
- 6 Messerschmidt, J., Macatangay, R., Notholt, J., Petri, C., Warneke, T., and Weinzierl, C.:  
7 Side by side measurements of CO<sub>2</sub> by ground-based Fourier transform spectrometry (FTS),  
8 Tellus B, 62, 749-758, doi:10.1111/j.1600-0889.2010.00491.x, 2010.
- 9
- 10 Miyamoto, Y., Inoue, M., Morino, I., Uchino, O., Yokota, T., Machida, T., Sawa, Y.,  
11 Matsueda, H., Sweeney, C., Tans, P. P., Andrews, A. E., Biraud, S. C., and Patra, P. K.:  
12 Atmospheric column-averaged mole fractions of carbon dioxide at 53 aircraft measurement  
13 sites, Atmos. Chem. Phys., 13, 5265-5275, doi:10.5194/acp-13-5265-2013, 2013.
- 14
- 15 Morino, I. Uchino, O., Inoue, M., Yoshida, Y., Yokota, T., Wennberg, P. O., Toon, G. C.,  
16 Wunch, D., Roehl, C. M., Notholt, J., Warneke, T., Messerschmidt, J., Griffith D. W. T.,  
17 Deutscher, N. M., Sherlock, V., Connor, B., Robinson, J., Sussmann, R., and Rettinger, M.:  
18 Preliminary validation of column-averaged volume mixing ratios of carbon dioxide and  
19 methane retrieved from GOSAT short-wavelength infrared spectra, Atmos. Meas. Tech., 4,  
20 1061-1076, doi:10.5194/amt-4-1061-2011, 2011.
- 21
- 22 Nakazawa, T., Sugawara, S., Inoue, G., Machida, T., Maksyutov, S., and Mukai, H.: Aircraft  
23 measurements of the concentrations of CO<sub>2</sub>, CH<sub>4</sub>, N<sub>2</sub>O, and CO and the carbon and oxygen  
24 isotopic ratios of CO<sub>2</sub> in the troposphere over Russia, J. Geophys. Res., 102, 3843-3859, 1997.
- 25
- 26 Nguyen, H., Osterman, G., Wunch, D., O'Dell, C., Mandrake, L., Wennberg, P., Fisher, B.,  
27 and Castano, R.: A method for collocating satellite XCO<sub>2</sub> data to ground-based data and its  
28 application to ACOS-GOSAT and TCCON, Atmos. Meas. Tech., 7, 2631-2644,  
29 doi:10.5194/amt-7-2631-2014, 2014.

30



- 1 O'Dell, C. W., Connor, B., Bösch, H., O'Brien, D., Frankenberg, C., Castano, R., Christi, M.,  
2 Eldering, D., Fisher, B., Gunson, M., McDuffie, J., Miller, C. E., Natraj, V., Oyafuso, F.,  
3 Polonsky, I., Smyth, M., Taylor, T., Toon, G. C., Wennberg, P. O., and Wunch, D.: The  
4 ACOS CO<sub>2</sub> retrieval algorithm – Part 1: Description and validation against synthetic  
5 observations, *Atmos. Meas. Tech.*, 5, 99-121, doi:10.5194/amt-5-99-2012, 2012.
- 6
- 7 Oshchepkov, S., Bril, A., Yokota, T., Wennberg, P. O., Deutscher, N. M., Wunch, D., Toon,  
8 G. C., Yoshida, Y., O'Dell, C. W., Crisp, D., Miller, C. E., Frankenberg, C., Butz, A., Aben, I.,  
9 Guerlet, S., Hasekamp, O., Boesch, H., Cogan, A., Parker, R., Griffith, D., Macatangay, R.,  
10 Notholt, J., Sussmann, R., Rettinger, M., Sherlock, V., Robinson, J., Kyrö, E., Heikkinen, P.,  
11 Feist, D. G., Morino, I., Kadyrov, N., Belikov, D., Maksyutov, S., Matsunaga, T., Uchino,  
12 O., and Watanabe, H.: Effects of atmospheric light scattering on spectroscopic observations of  
13 greenhouse gases from space. Part 2: Algorithm intercomparison in the GOSAT data  
14 processing for CO<sub>2</sub> retrievals over TCCON sites, *J. Geophys. Res.*, 118, 1493-1512,  
15 doi:10.1002/jgrd.50146, 2013.
- 16
- 17 Saito, R., Patra, P. K., Deutscher, N., Wunch, D., Ishijima, K., Sherlock, V., Blumenstock, T.,  
18 Dohe, S., Griffith, D., Hase, F., Heikkinen, P., Kyrö, E., Macatangay, R., Mendonca, J.,  
19 Messerschmidt, J., Morino, I., Notholt, J., Rettinger, M., Strong, K., Sussmann, R., and  
20 Warneke, T.: Technical Note: Latitude-time variations of atmospheric column-average dry air  
21 mole fractions of CO<sub>2</sub>, CH<sub>4</sub> and N<sub>2</sub>O, *Atmos. Chem. Phys.*, 12, 7767-7777, doi:10.5194/acp-  
22 12-7767-2012, 2012.
- 23
- 24 Saitoh, N., Touno, M., Hayashida, S., Imasu, R., Shiomi, K., Yokota, T., Yoshida, Y.,  
25 Machida, T., Matsueda, H., and Sawa, Y.: Comparisons between XCH<sub>4</sub> from GOSAT  
26 Shortwave and Thermal Infrared Spectra and Aircraft CH<sub>4</sub> Measurement over Guam, *Sci.*  
27 *Online Lett. Atmos. (SOLA)*, 8, 145-149, doi:10.2151/sola.2012-036, 2012.
- 28
- 29 Santoni, G. W., Daube, B. C., Kort, E. A., Jiménez, R., Park, S., Pittman, J. V., Gottlieb, E.,  
30 Xiang, B., Zahniser, M. S., Nelson, D. D., McManus, J. B., Peischl, J., Ryerson, T. B.,  
31 Holloway, J. S., Andrews, A. E., Sweeney, C., Hall, B., Hintsa, E. J., Moore, F. L., Elkins, J.



- 1 W., Hurst, D. F., Stephens, B. B., Bent, J., and Wofsy, S. C.: Evaluation of the airborne  
2 quantum cascade laser spectrometer (QCLS) measurements of the carbon and greenhouse gas  
3 suite – CO<sub>2</sub>, CH<sub>4</sub>, N<sub>2</sub>O, and CO – during the CalNex and HIPPO campaigns, Atmos. Meas.  
4 Tech., 7, 1509-1526, doi:10.5194/amt-7-1509-2014, 2014.
- 5
- 6 Scheepmaker, R. A., Frankenberg, C., Deutscher, N. M., Schneider, M., Barthlott, S.,  
7 Blumenstock, T., Garcia, O. E., Hase, F., Jones, N., Mahieu, E., Notholt, J., Velazco, V.,  
8 Landgraf, J., and Aben, I.: Validation of SCIAMACHY HDO/H<sub>2</sub>O measurements using the  
9 TCCON and NDACC-MUSICA networks, Atmos. Meas. Tech., 8, 1799-1818,  
10 doi:10.5194/amt-8-1799-2015, 2015.
- 11
- 12 Schmid, B., Tomlinson, J. M., Hubbe, J. M., Comstock, J. M., Mei, F., Chand, D., Pekour, M.  
13 S., Kluzek, C. D., Andrews, E., Biraud, S. C., and McFarquhar, G. M.: The DOE ARM Aerial  
14 Facility. Bull. Amer. Meteor. Soc., 95, 723-742, doi:10.1175/BAMS-D-13-00040.1, 2014.
- 15
- 16 Schneising, O., Bergamaschi, P., Bovensmann, H., Buchwitz, M., Burrows, J. P., Deutscher,  
17 N. M., Griffith, D. W. T., Heymann, J., Macatangay, R., Messerschmidt, J., Notholt, J.,  
18 Rettinger, M., Reuter, M., Sussmann, R., Velazco, V. A., Warneke, T., Wennberg, P. O., and  
19 Wunch, D.: Atmospheric greenhouse gases retrieved from SCIAMACHY: comparison to  
20 ground-based FTS measurements and model results, Atmos. Chem. Phys., 12, 1527-1540,  
21 doi:10.5194/acp-12-1527-2012, 2012.
- 22
- 23 Schneising, O., Heymann, J., Buchwitz, M., Reuter, M., Bovensmann, H., and Burrows, J. P.:  
24 Anthropogenic carbon dioxide source areas observed from space: assessment of regional  
25 enhancements and trends, Atmos. Chem. Phys., 13, 2445-2454, doi:10.5194/acp-13-2445-  
26 2013, 2013.
- 27
- 28 Sweeney, C., Karion, A., Wolter, S., Newberger, T., Guenther, D., Higgs, J. A., Andrews, A.  
29 E., Lang, P. M., Neff, D., Dlugokencky, E., Miller, J. B., Montzka, S. A., Miller, B. R.,  
30 Masarie, K. A., Biraud, S. C., Novelli, P. C., Crotwell, M., Crotwell, A. M., Thoning, K., and



- 1 Tans, P. P.: Seasonal climatology of CO<sub>2</sub> across North America from aircraft measurements  
2 in the NOAA/ESRL Global Greenhouse Gas Reference Network, *J. Geophys. Res.*, 120,  
3 5155-5190, doi:10.1002/2014JD022591, 2015.
- 4
- 5 Takagi, H., Saeki, T., Oda, T., Saito, M., Valsala, V., Belikov, D., Saito, R., Yoshida, Y.,  
6 Morino, I., Uchino, O., Andres, R. J., Yokota T., and Maksyutov, S.: On the Benefit of  
7 GOSAT Observations to the Estimation of Regional CO<sub>2</sub> Fluxes, *Sci. Online Lett. Atmos.*  
8 (SOLA), 7, 161-164, doi:10.2151/sola.2011-041, 2011.
- 9
- 10 Tanaka, T., Miyamoto, Y., Morino, I., Machida, T., Nagahama, T., Sawa, Y., Matsueda, H.,  
11 Wunch, D., Kawakami, S., and Uchino, O.: Aircraft measurements of carbon dioxide and  
12 methane for the calibration of ground-based high-resolution Fourier Transform Spectrometers  
13 and a comparison to GOSAT data measured over Tsukuba and Moshiri, *Atmos. Meas. Tech.*,  
14 5, 2003-2012, doi:10.5194/amt-5-2003-2012, 2012.
- 15
- 16 Tsuboi, K., Matsueda, H., Sawa, Y., Niwa, Y., Nakamura, M., Kuboike, D., Saito, K., Ohmori,  
17 H., Iwatsubo, S., Nishi, H., Hanamiya, Y., Tsuji, K., and Baba, Y.: Evaluation of a new JMA  
18 aircraft flask sampling system and laboratory trace gas analysis system, *Atmos. Meas. Tech.*,  
19 6, 1257-1270, doi:10.5194/amt-6-1257-2013, 2013.
- 20
- 21 Uchino, O., Kikuchi, N., Sakai, T., Morino, I., Yoshida, Y., Nagai, T., Shimizu, A., Shibata,  
22 T., Yamazaki, A., Uchiyama, A., Kikuchi, N., Oshchepkov, S., Bril, A., and Yokota, T.:  
23 Influence of aerosols and thin cirrus clouds on the GOSAT-observed CO<sub>2</sub>: a case study over  
24 Tsukuba, *Atmos. Chem. Phys.*, 12, 3393-3404, doi:10.5194/acp-12-3393-2012, 2012.
- 25
- 26 WMO: WMO Greenhouse Gas Bulletin, The State of Greenhouse Gases in the Atmosphere  
27 Using Global Observations through 2007, No. 4, World Meteorological Organization, 2008,  
28 available at: <http://www.wmo.int/pages/prog/arep/gaw/ghg/GHGbulletin.html> (last access:  
29 January 2015).
- 30



1 WMO: WMO Greenhouse Gas Bulletin, The State of Greenhouse Gases in the Atmosphere  
2 Based on Global Observations through 2013, No. 10, World Meteorological Organization,  
3 2014, available at: <http://www.wmo.int/pages/prog/arep/gaw/ghg/GHGbulletin.html> (last  
4 access: January 2015).

5

6 Wofsy, S. C. and the HIPPO Science Team and Cooperating Modellers and Satellite Teams:  
7 HIAPER Pole-to-Pole Observations (HIPPO): fine-grained, global-scale measurements of  
8 climatically important atmospheric gases and aerosols, *Philos. T. Roy. Soc. A*, 369, 2073-  
9 2086, doi:10.1098/rsta.2010.0313, 2011.

10

11 Wofsy, S. C., Daube, B. C., Jimenez, R., Kort, E., Pittman, J. V., Park, S., Commane, R.,  
12 Xiang, B., Santoni, G., Jacob, D., Fisher, J., Pickett-Heaps, C., Wang, H., Wecht, K., Wang,  
13 Q.-Q., Stephens, B. B., Shertz, S., Watt, A. S., Romashkin, P., Campos, T., Haggerty, J.,  
14 Cooper, W. A., Rogers, D., Beaton, S., Hendershot, R., Elkins, J. W., Fahey, D. W., Gao, R.  
15 S., Moore, F., Montzka, S. A., Schwarz, J. P., Perring, A. E., Hurst, D., Miller, B. R.,  
16 Sweeney, C., Oltmans, S., Nance, D., Hints, E., Dutton, G., Watts, L. A., Spackman, J. R.,  
17 Rosenlof, K. H., Ray, E. A., Hall, B., Zondlo, M. A., Diao, M., Keeling, R., Bent, J., Atlas, E.  
18 L., Lueb, R., and Mahoney, M. J.: HIPPO merged 10-second Meteorology, Atmospheric  
19 Chemistry, Aerosol Data (R\_20121129), used data file  
20 “HIPPO\_all\_missions\_merged\_10s\_20121129.tbl”, Carbon Dioxide Information Analysis  
21 Center, Oak Ridge National Laboratory, Oak Ridge, Tennessee, U.S.A.  
22 [http://dx.doi.org/10.3334/CDIAC/hippo\\_010](http://dx.doi.org/10.3334/CDIAC/hippo_010), (last access: July 2013), 2012.

23

24 Wunch, D., Wennberg, P. O., Toon, G. C., Keppel-Aleks, G., and Yavin, Y. G.: Emissions of  
25 greenhouse gases from a North American megacity, *Geophys. Res. Lett.*, 36, L15810,  
26 doi:10.1029/2009GL039825, 2009.

27

28 Wunch, D., Toon, G. C., Wennberg, P. O., Wofsy, S. C., Stephens, B. B., Fischer, M. L.,  
29 Uchino, O., Abshire, J. B., Bernath, P., Biraud, S. C., Blavier, J.-F. L., Boone, C., Bowman, K.  
30 P., Browell, E. V., Campos, T., Connor, B. J., Daube, B. C., Deutscher, N. M., Diao, M.,  
31 Elkins, J. W., Gerbig, C., Gottlieb, E., Griffith, D. W. T., Hurst, D. F., Jiménez, R., Keppel-





- 1 Aleks, G., Kort, E. A., Macatangay, R., Machida, T., Matsueda, H., Moore, F., Morino, I.,  
2 Park, S., Robinson, J., Roehl, C. M., Sawa, Y., Sherlock, V., Sweeney, C., Tanaka, T., and  
3 Zondlo, M. A.: Calibration of the Total Carbon Column Observing Network using aircraft  
4 profile data, *Atmos. Meas. Tech.*, 3, 1351-1362, doi:10.5194/amt-3-1351-2010, 2010.
- 5
- 6 Wunch, D., Toon, G. C., Blavier, J.-F. L., Washenfelder, R. A., Notholt, J., Connor, B. J.,  
7 Griffith, D. W. T., Sherlock, V., and Wennberg, P. O.: The Total Carbon Column Observing  
8 Network, *Phil. Trans. R. Soc. A*, 369, 2087-2112, doi:10.1098/rsta.2010.0240, 2011a.
- 9
- 10 Wunch, D., Wennberg, P. O., Toon, G. C., Connor, B. J., Fisher, B., Osterman, G. B.,  
11 Frankenberg, C., Mandrake, L., O'Dell, C., Ahonen, P., Biraud, S. C., Castano, R., Cressie,  
12 N., Crisp, D., Deutscher, N. M., Eldering, A., Fisher, M. L., Griffith, D. W. T., Gunson, M.,  
13 Heikkinen, P., Keppel-Aleks, G., Kyrö, E., Lindenmaier, R., Macatangay, R., Mendonca, J.,  
14 Messerschmidt, J., Miller, C. E., Morino, I., Notholt, J., Oyafuso, F. A., Rettinger, M.,  
15 Robinson, J., Roehl, C. M., Salawitch, R. J., Sherlock, V., Strong, K., Susmann, R., Tanaka,  
16 T., Thompson, D. R., Uchino, O., Warneke, T., and Wofsy, S. C.: A method for evaluating  
17 bias in global measurements of CO<sub>2</sub> total columns from space, *Atmos. Chem. Phys.*, 11,  
18 12317-12337, doi:10.5194/acp-11-12317-2011, 2011b.
- 19
- 20 Wunch, D., Toon, G. C., Sherlock, V., Deutscher, N. M., Liu, X., Feist, D. G., and Wennberg,  
21 P. O.: The Total Carbon Column Observing Network's GGG2014 Data Version. Carbon  
22 Dioxide Information Analysis Center, Oak Ridge National Laboratory, Oak Ridge, Tennessee,  
23 U.S.A. doi: 10.14291/tcon.ggg2014.documentation.R0/1221662, 2015.
- 24
- 25 Xiong, X., Barnet, C., Maddy, E., Sweeney, C., Liu, X., Zhou, L., and Goldberg, M.:  
26 Characterization and validation of methane products from the Atmospheric Infrared Sounder  
27 (AIRS), *J. Geophys. Res.*, 113, G00A01, doi:10.1029/2007JG000500, 2008.
- 28



- 1 Yokota, T., Yoshida, Y., Eguchi, N., Ota, Y., Tanaka, T., Watanabe, H., and Maksyutov, S.:  
2 Global Concentrations of CO<sub>2</sub> and CH<sub>4</sub> Retrieved from GOSAT: First Preliminary Results,  
3 Sci. Online Lett. Atmos. (SOLA), 5, 160-163, doi:10.2151/sola.2009-041, 2009.  
4
- 5 Yoshida, Y., Ota, Y., Eguchi, N., Kikuchi, N., Nobuta, K., Tran, H., Morino, I., and Yokota,  
6 T.: Retrieval algorithm for CO<sub>2</sub> and CH<sub>4</sub> column abundances from short-wavelength infrared  
7 spectral observations by the Greenhouse gases observing satellite, Atmos. Meas. Tech., 4,  
8 717-734, doi:10.5194/amt-4-717-2011, 2011.  
9
- 10 Yoshida, Y., Kikuchi, N., Morino, I., Uchino, O., Oshchepkov, S., Bril, A., Saeki, T.,  
11 Schutgens, N., Toon, G. C., Wunch, D., Roehl, C. M., Wennberg, P. O., Griffith, D. W. T.,  
12 Deutscher, N. M., Warneke, T., Notholt, J., Robinson, J., Sherlock, V., Connor, B., Rettinger,  
13 M., Sussmann, R., Ahonen, P., Heikkinen, P., Kyrö, E., Mendonca, J., Strong, K., Hase, F.,  
14 Dohe, S., and Yokota, T.: Improvement of the retrieval algorithm for GOSAT SWIR XCO<sub>2</sub>  
15 and XCH<sub>4</sub> and their validation using TCCON data, Atmos. Meas. Tech., 6, 1533-1547,  
16 doi:10.5194/amt-6-1533-2013, 2013.  
17



1 Table 1. Basic information on the TCCON sites used for correction and validation of the  
 2 GOSAT data.

3

site	latitude [deg. N]	longitude [deg. E]	elevation [m]	region	data reference (DOI number)
Ny Ålesund	78.90	11.90	20	Spitzbergen, Norway	10.14291/tcon.ggg2014. nyalesund01.R0/1149278
Sodankylä	67.37	26.63	188	Finland	10.14291/tcon.ggg2014. sodankyla01.R0/1149280
Białystok	53.23	23.03	180	Poland	10.14291/tcon.ggg2014. bialystok01.R1/1183984
Bremen	53.10	8.85	27	Germany	10.14291/tcon.ggg2014. bremen01.R0/1149275
Karlsruhe	49.10	8.44	120	Germany	10.14291/tcon.ggg2014. karlsruhe01.R1/1182416
Orléans	47.97	2.11	130	France	10.14291/tcon.ggg2014. orleans01.R0/1149276
Garmisch	47.48	11.06	740	Germany	10.14291/tcon.ggg2014. garmisch01.R0/1149299
Park Falls	45.95	-90.27	472	United States	10.14291/tcon.ggg2014. parkfalls01.R0/1149161
Rikubetsu	43.46	143.77	361	Japan	10.14291/tcon.ggg2014. rikubetsu01.R0/1149282
Indianapolis	39.86	-86.00	270	United States	10.14291/tcon.ggg2014. indianapolis01.R0/1149164
Four Corners	36.80	-108.48	1643	United States	10.14291/tcon.ggg2014. fourcorners01.R0/1149272
Lamont	36.60	-97.49	320	United States	10.14291/tcon.ggg2014. lamont01.R0/1149159
Tsukuba	36.05	140.12	30	Japan	(120HR) 10.14291/tcon.ggg2014. tsukuba01.R0/1149281
					(125HR) 10.14291/tcon.ggg2014. tsukuba02.R0/1149301
Edwards	34.96	-117.88	700	United States	10.14291/tcon.ggg2014. edwards01.R0/1149289
JPL	34.20	-118.18	390	United States	10.14291/tcon.ggg2014. jpl02.R0/1149297
Pasadena	34.14	-118.13	237	United States	10.14291/tcon.ggg2014. pasadena01.R1/1182415
Saga	33.24	130.29	7	Japan	10.14291/tcon.ggg2014. saga01.R0/1149283
Izaña	28.30	-16.50	2370	Tenerife, Canary Islands	10.14291/tcon.ggg2014. izana01.R0/1149295
Ascension Island	-7.92	-14.33	31	South Atlantic Ocean	10.14291/tcon.ggg2014. ascension01.R0/1149285
Darwin	-12.42	130.89	30	Australia	10.14291/tcon.ggg2014. darwin01.R0/1149290



Reunion Island	-20.90	55.49	87	Indian Ocean	10.14291/tcon.ggg2014. reunion01.R0/1149288
Wollongong	-34.41	150.88	30	Australia	10.14291/tcon.ggg2014. wollongong01.R0/1149291 (120HR)
Lauder	-45.04	169.68	370	New Zealand	10.14291/tcon.ggg2014. lauder01.R0/1149293 (125HR)
					10.14291/tcon.ggg2014. lauder02.R0/1149298

1  
2  
3  
4  
5  
6  
7  
8  
9  
10  
11  
12  
13  
14  
15  
16  
17  
18  
19



- 1 Table 2. Basic information on the aircraft observation sites used for validation of the GOSAT
- 2 data.

(a) CONTRAIL

site code	latitude [deg. N]	longitude [deg. E]	elevation [m]	region	site name
LHR	51.5	-0.5	24	London	Heathrow Airport
YVR	49.2	-123.2	4	Vancouver	Vancouver International Airport
MXP	45.6	8.7	24	Milan	Milan Malpensa International Airport
FCO	41.8	12.3	5	Rome	Fiumicino Airport
ICN	37.5	126.5	7	Incheon	Incheon International Airport
NRT	35.8	140.4	43	Narita	Narita International Airport
HND	35.6	139.8	6	Haneda	Tokyo International Airport
NGO	34.9	136.8	5	Nagoya	Chubu Centrair International Airport
KIX	34.4	135.2	0	Kansai	Kansai International Airport
HNL	21.3	-157.9	4	Honolulu	Honolulu International Airport
BKK	13.7	100.7	2	Bangkok	Suvarnabhumi International Airport
SIN	1.4	104.0	7	Singapore	Singapore Changi International Airport
CGK	-6.1	106.7	10	Jakarta	Jakarta International Soekarno-Hatta Airport
SYD	-33.9	151.2	6	Sydney	Kingsford Smith Airport

(b) NOAA

site code	latitude [deg. N]	longitude [deg. E]	elevation [m]	region	site name
DND	48.4	-97.8	464	United States	Dahlen, North Dakota
LEF	45.9	-90.3	472	United States	Park Falls, Wisconsin
NHA	43.0	-70.6	0	United States	Worcester, Massachusetts
WBI	41.7	-91.4	242	United States	West Branch, Iowa
THD	41.1	-124.2	107	United States	Trinidad Head, California
BNE	40.8	-97.2	466	United States	Beaver Crossing, Nebraska
CAR	40.4	-104.3	1740	United States	Briggsdale, Colorado
HIL	40.1	-87.9	202	United States	Homer, Illinois
AAO	40.1	-88.6	213	United States	Airborne Aerosol Observing, Illinois
SCA	32.8	-79.6	0	United States	Charleston, South Carolina
TGC	27.7	-96.9	0	United States	Sinton, Texas



RTA	-21.3	-159.8	3	Cook Islands	Rarotonga
-----	-------	--------	---	--------------	-----------

(c) DOE

site code	latitude [deg. N]	longitude [deg. E]	elevation [m]	region	site name
SGP	36.8	-97.5	314	United States	Southern Great Plains, Oklahoma

(d) NIES

site code	latitude [deg. N]	longitude [deg. E]	elevation [m]	region	site name
YAK	62	130	136	Russia	Yakutsk
SGM	35.1	139.3	0	Japan	Sagami-bay

(e) JMA

site code	latitude [deg. N]	longitude [deg. E]	elevation [m]	region	site name
MNM	24.3	154.0	8	Japan	Minamitorishima

1

(f) HIPPO

site code	latitude [deg. N]	longitude [deg. E]	elevation [m]	region	site name
HPA	49	-110	1040	United States	northeastern part of Great Falls, Montana
HPB	-28	-166	0	South Pacific Ocean	southwestern part of Rarotonga
HPC	-23	-161	0	South Pacific Ocean	southwestern part of Rarotonga
HPD	-33	158	0	Australia	eastern part of Lord Howe
HPE	-33	152	0	Australia	east coast of Newcastle
HPF	-20	156	0	Coral Sea	western part of Chesterfield Islands
HPG	-5	-167	0	Kiribati	western part of Enderbury
HPH	-37	179	0	New Zealand	northeastern part of Bay of Plenty
HPI	-36	179	0	New Zealand	northeastern part of Bay of Plenty

2

(g)  
 NIES-JAXA

site code	latitude [deg. N]	longitude [deg. E]	elevation [m]	region	site name
TKB	36.1	140.1	31	Japan	Tsukuba



1 Table 3. Values and errors of the regression coefficients for (a) XCO<sub>2</sub> and (b) XCH<sub>4</sub> retrievals  
 2 calculated by multiple linear regression. The units of C<sub>0</sub>, C<sub>1</sub>, C<sub>2</sub>, C<sub>3</sub>, and C<sub>4</sub> for XCO<sub>2</sub> are  
 3 [ppm], [ppm/units of AOD], [ppm/hPa], [ppm/airmass], and [ppm/units of albedo],  
 4 respectively. The units of C<sub>0</sub> and C<sub>1</sub> for XCH<sub>4</sub> are [ppb] and [ppb/units of AOD], respectively.

5

(a)

6

XCO <sub>2</sub> coefficients	Land		Ocean	
	Values	Errors	Values	Errors
C <sub>0</sub>	0.865	0.021	1.903	0.055
C <sub>1</sub>	-7.793	1.357	15.493	2.725
C <sub>2</sub>	-0.282	0.006	-0.237	0.013
C <sub>3</sub>	0.023	0.064	8.602	1.060
C <sub>4</sub>	-2.036	0.433	—	—

7

8

(b)

9

XCH <sub>4</sub>	Land		Ocean	
	Values	Errors	Values	Errors
C <sub>0</sub>	6.0	0.2	0.2	0.6
C <sub>1</sub>	45.8	10.0	103.0	26.4

10

11

12



1 Table 4. The average and standard deviation of the differences between uncorrected/corrected  
 2 GOSAT XCO<sub>2</sub> and TCCON XCO<sub>2</sub> at each TCCON site. The GOSAT data were retrieved  
 3 over (a) land and (b) ocean regions within ±5° latitude/longitude boxes centered at each site.  
 4 The averages and standard deviations of the differences of the matched data at all TCCON  
 5 sites (single scan) and those of the station biases are also shown in the second row from the  
 6 bottom and the bottom row of the table, respectively.

7  
 8

(a)

Land		Differences between uncorrected XCO <sub>2</sub> and TCCON XCO <sub>2</sub>		Differences between corrected GOSAT XCO <sub>2</sub> and TCCON XCO <sub>2</sub>	
site	number	average [ppm]	SD [ppm]	average [ppm]	SD [ppm]
Sodankylä	152	-0.03	1.93	0.48	1.92
Białystok	305	-0.18	2.22	0.79	2.05
Bremen	62	-0.10	1.98	0.46	1.52
Karlsruhe	229	0.35	2.27	0.85	2.01
Orléans	402	-0.26	2.00	0.24	1.82
Garmisch	326	0.23	2.42	0.70	2.17
Park Falls	482	-0.50	2.15	0.37	1.90
Rikubetsu	7	-0.92	1.32	-0.46	0.84
Indianapolis	158	-0.03	1.69	0.37	1.37
Four Corners	142	-1.17	1.95	0.07	1.87
Lamont	2767	-1.72	1.79	-0.49	1.61
Tsukuba	419	1.55	2.37	1.67	2.24
Edwards	38	-1.35	1.46	-0.49	1.10
JPL	264	-2.32	2.32	-1.01	2.33
Pasadena	109	-0.41	2.12	0.22	2.45
Saga	128	0.37	2.37	0.66	2.31
Izaña	56	0.47	1.34	0.92	1.04
Darwin	926	-1.16	1.51	-0.25	1.34
Wollongong	1071	-0.68	2.25	-0.05	2.25
Lauder	202	-0.77	1.79	-0.23	1.83
Total (single scan)	8245	-0.86	2.18	0.00	1.94
Total (station bias)	20	-0.43	0.87	0.24	0.62





1  
 2  
 3  
 4  
 5  
 6  
 7  
 8  
 9  
 10  
 11  
 12  
 13  
 14

(b)

Ocean		Differences between uncorrected XCO <sub>2</sub> and TCCON XCO <sub>2</sub>		Differences between corrected GOSAT XCO <sub>2</sub> and TCCON XCO <sub>2</sub>	
site	number	average [ppm]	SD [ppm]	average [ppm]	SD [ppm]
Garmisch	5	-0.55	0.49	-0.67	0.83
Tsukuba	2	-2.87	2.35	-4.01	0.65
JPL	8	-4.71	3.64	-1.36	2.47
Saga	14	-1.15	2.56	-0.34	1.56
Izana	50	-1.50	1.36	0.23	1.17
Ascension Island	234	-1.93	1.62	-0.17	1.18
Darwin	85	-1.64	1.86	0.54	1.56
Reunion Island	43	-2.19	1.43	-0.08	0.95
Wollongong	97	-2.04	1.49	0.05	1.04
Lauder	6	-2.54	2.32	0.53	0.87
Total (single scan)	544	-1.90	1.72	-0.01	1.29
Total (station bias)	10	-2.11	1.13	-0.53	1.35



1 Table 5. The average and standard deviation of the differences between uncorrected/corrected  
 2 GOSAT XCH<sub>4</sub> and TCCON XCH<sub>4</sub> at each TCCON site. The GOSAT data were retrieved  
 3 over (a) land and (b) ocean regions within ±5° latitude/longitude boxes centered at each site.  
 4 The averages and standard deviations of the differences of the matched data at all TCCON  
 5 sites (single scan) and those of the station biases are also shown in the second row from the  
 6 bottom and the bottom row of the table, respectively.

7  
 8

(a)

Land		Differences between uncorrected GOSAT XCH <sub>4</sub> and TCCON XCH <sub>4</sub>		Differences between corrected GOSAT XCH <sub>4</sub> and TCCON XCH <sub>4</sub>	
site	number	average [ppb]	SD [ppb]	average [ppb]	SD [ppb]
Sodankylä	152	-2.3	11.4	3.8	11.4
Białystok	305	0.5	12.9	6.2	12.9
Bremen	62	-1.6	12.7	4.2	12.7
Karlsruhe	229	-0.9	15.3	5.0	15.3
Orléans	402	-3.9	12.7	2.0	12.7
Garmisch	326	6.2	16.3	11.9	16.3
Park Falls	482	3.3	13.9	9.2	13.9
Rikubetsu	7	4.1	8.6	9.7	8.8
Indianapolis	158	-1.4	10.9	5.0	10.9
Four Corners	142	-8.9	14.2	-3.0	14.3
Lamont	2767	-9.0	15.1	-2.9	15.2
Tsukuba	419	1.9	13.2	7.5	13.1
Edwards	38	-19.5	16.8	-13.2	16.7
JPL	264	-21.1	19.4	-15.1	19.4
Pasadena	109	-8.1	15.3	-1.8	15.3
Saga	128	-5.3	14.4	0.0	14.4
Izana	56	15.4	12.7	20.1	13.1
Darwin	926	-8.6	8.9	-2.4	9.1
Wollongong	1076	-9.1	14.5	-2.8	14.7
Lauder	208	-3.9	11.3	2.4	11.2
Total (single scan)	8256	-6.0	15.2	0.0	15.2
Total (station bias)	20	-3.6	8.4	2.3	8.1

9



1  
 2  
 3

(b)

Ocean		Differences between uncorrected XCH <sub>4</sub> and TCCON XCH <sub>4</sub>		Differences between corrected GOSAT XCH <sub>4</sub> and TCCON XCH <sub>4</sub>	
site	number	average [ppb]	SD [ppb]	average [ppb]	SD [ppb]
Garmisch	5	18.7	11.0	20.4	11.0
Tsukuba	2	21.9	16.0	21.2	17.2
JPL	8	-17.1	13.1	-17.4	12.9
Saga	14	0.7	17.0	-0.3	17.0
Izana	50	14.8	7.7	14.1	8.4
Ascension Island	234	-1.0	11.5	-0.6	11.2
Darwin	85	4.1	13.2	3.0	13.3
Reunion Island	43	-0.4	8.3	0.1	8.9
Wollongong	97	-9.7	11.1	-8.6	11.7
Lauder	6	-5.9	11.9	-4.3	12.3
Total (single scan)	544	-0.2	13.4	-0.1	13.2
Total (station bias)	10	2.6	12.6	2.8	12.5

4  
 5  
 6  
 7  
 8  
 9  
 10  
 11  
 12  
 13



1 Table 6. The average and standard deviation of the differences between uncorrected/corrected  
 2 GOSAT XCO<sub>2</sub> and aircraft-based XCO<sub>2</sub> at each aircraft observation site. The GOSAT data  
 3 were retrieved over (a) land and (b) ocean regions within ±5° latitude/longitude boxes  
 4 centered at each site. The averages and standard deviations of the differences of the matched  
 5 data at all aircraft observation sites (single scan) and those of the station biases are also shown  
 6 in the second row from the bottom and the bottom row of the table, respectively.

7  
 8  
 9  
 10

(a)

Land		Differences between uncorrected XCO <sub>2</sub> and aircraft-based XCO <sub>2</sub>		Differences between corrected GOSAT XCO <sub>2</sub> and aircraft-based XCO <sub>2</sub>	
Site	number	average [ppm]	SD [ppm]	average [ppm]	SD [ppm]
LHR	3	-3.24	1.25	-2.09	0.66
YVR	7	-0.64	2.07	0.21	1.95
MXP	2	0.06	1.88	1.09	1.54
ICN	1	0.64	—	3.37	—
NRT	69	0.17	2.52	0.54	2.34
HND	2	-0.38	2.56	0.09	3.83
NGO	15	0.27	2.47	0.73	2.39
KIX	5	-1.01	3.25	-0.19	2.73
BKK	5	-2.90	3.86	-1.78	3.43
SYD	22	-1.19	2.48	-0.62	2.19
DND	11	-1.37	1.74	-0.47	1.48
LEF	34	0.02	2.77	0.66	2.79
NHA	25	0.27	1.64	0.44	1.69
WBI	23	-0.95	2.92	0.17	2.43
THD	4	-1.99	1.64	-0.06	1.13
BNE	6	-1.15	2.48	0.15	2.02
CAR	51	-2.17	2.20	-0.73	1.93
HIL	37	-2.16	1.96	-1.25	2.33
AAO	20	-0.18	2.32	0.64	2.28



SCA	22	-0.31	1.56	-0.01	1.60
TGC	15	-0.51	2.53	0.45	3.02
SGP	68	-1.61	2.20	-0.43	2.03
YAK	3	1.70	2.89	1.79	2.59
SGM	6	1.02	3.11	1.63	2.71
HPA	1	-2.84	—	-0.76	—
HPH	1	-1.91	—	-0.71	—
TKB	11	0.11	1.89	0.17	1.68
Total (single scan)	469	-0.85	2.48	-0.04	2.28
Total (station bias)	27	-0.82	1.24	0.11	1.11

1  
 2  
 3  
 4

(b)

Ocean		Differences between uncorrected XCO <sub>2</sub> and aircraft-based XCO <sub>2</sub>		Differences between corrected GOSAT XCO <sub>2</sub> and aircraft-based XCO <sub>2</sub>	
site	number	average [ppm]	SD [ppm]	average [ppm]	SD [ppm]
FCO	1	0.12	—	-3.39	—
NRT	4	-4.27	3.24	-2.89	2.49
HND	1	0.86	—	2.51	—
NGO	3	-1.43	0.77	-0.02	0.58
KIX	4	-3.00	1.95	-1.86	1.56
HNL	19	-1.49	1.06	0.66	1.36
BKK	2	-3.40	0.96	-1.10	0.24
SIN	4	-2.33	1.70	0.06	2.05
CGK	2	-2.46	3.12	0.57	0.25
SYD	5	-1.52	1.28	-0.03	1.04
NHA	3	-1.56	1.07	-1.60	2.06
SCA	5	-2.67	2.05	-0.45	1.99
TGC	2	-2.36	0.12	-0.52	0.02



RTA	6	-2.93	1.75	-0.39	1.36
MNM	3	-1.39	0.61	-0.45	1.41
HPB	1	-0.16	—	0.86	—
HPD	1	-2.21	—	0.07	—
HPG	1	-3.29	—	-1.89	—
Total (single scan)	67	-2.08	1.69	-0.32	1.74
Total (station bias)	18	-1.97	1.31	-0.55	1.41

1

2

3

4

5

6

7

8

9

10

11

12

13

14

15

16

17

18



1 Table 7. The average and standard deviation of the differences between uncorrected/corrected  
 2 GOSAT XCH<sub>4</sub> and aircraft-based XCH<sub>4</sub> at each aircraft observation site. The GOSAT data  
 3 were retrieved over (a) land and (b) ocean regions within ±5° latitude/longitude boxes  
 4 centered at each site. The averages and standard deviations of the differences of the matched  
 5 data at all aircraft observation sites (single scan) and those of the station biases are also shown  
 6 in the second row from the bottom and the bottom row of the table, respectively.

7

(a)		Differences between uncorrected GOSAT XCH <sub>4</sub> and aircraft-based XCH <sub>4</sub>		Differences between corrected GOSAT XCH <sub>4</sub> and aircraft-based XCH <sub>4</sub>	
site	number	average [ppb]	SD [ppb]	average [ppb]	SD [ppb]
DND	12	7.3	10.0	5.0	10.0
LEF	33	9.3	19.9	7.1	19.8
NHA	26	7.4	14.6	5.2	14.4
WBI	19	5.3	12.7	2.7	13.2
THD	4	-15.6	20.3	-17.9	20.6
BNE	5	9.4	9.1	7.0	9.0
CAR	44	5.6	13.7	3.2	14.1
HIL	32	2.6	14.3	0.1	14.2
AAO	21	0.6	15.4	-2.1	15.3
SCA	20	7.9	12.4	5.9	12.4
TGC	13	8.7	16.2	6.7	16.4
SGP	69	0.4	15.7	-1.8	15.8
YAK	8	3.0	17.6	0.4	17.5
SGM	7	2.7	9.4	-0.3	9.3
HPA	1	-10.6	—	-12.5	—
HPI	1	3.0	—	1.5	—
TKB	11	10.8	12.4	8.5	12.0
Total (single scan)	326	4.5	15.2	2.2	15.3
Total (station bias)	17	3.4	7.0	1.1	7.0

8



1  
 2  
 3  
 4  
 5

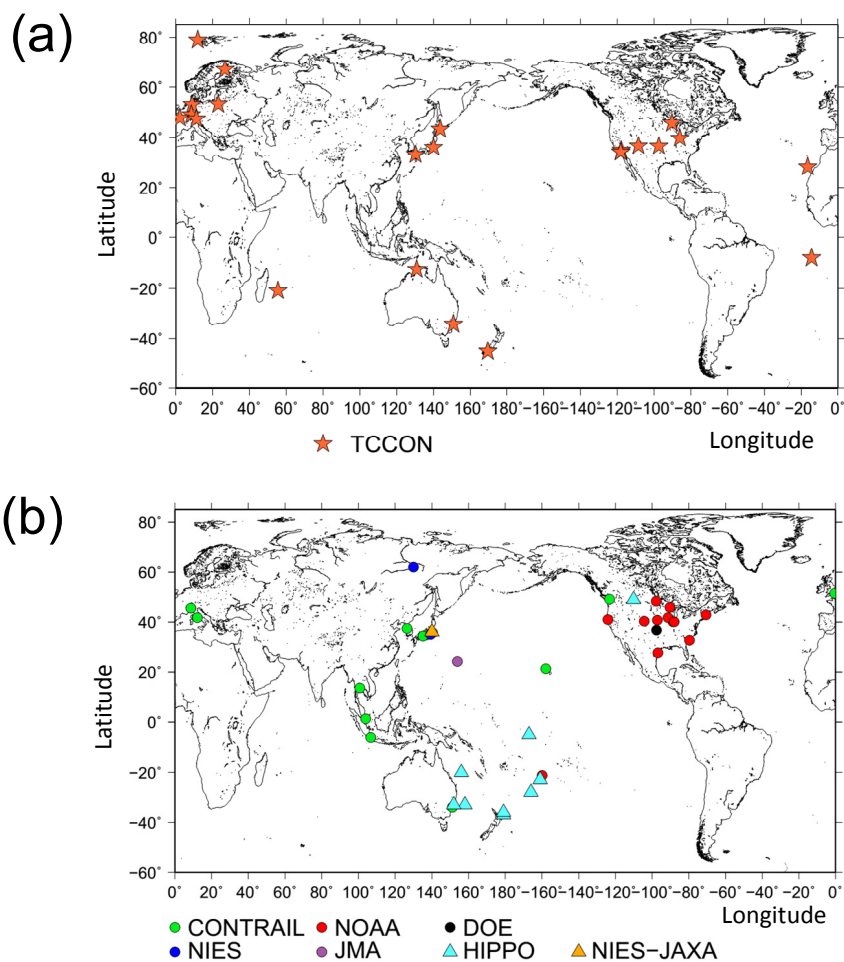
(b)

Ocean		Differences between uncorrected XCH <sub>4</sub> and aircraft-based XCH <sub>4</sub>		Differences between corrected GOSAT XCH <sub>4</sub> and aircraft-based XCH <sub>4</sub>	
site	number	average [ppb]	SD [ppb]	average [ppb]	SD [ppb]
NHA	3	24.2	10.9	16.7	10.1
SCA	5	-4.9	9.1	-13.6	9.6
TGC	2	9.5	2.3	3.1	2.8
RTA	7	5.2	14.5	-3.0	15.2
MNM	4	13.1	8.2	3.6	8.0
HPC	1	-2.2	—	-7.9	—
HPE	1	7.5	—	1.4	—
HPF	1	4.9	—	-3.5	—
HPG	1	-0.2	—	-13.8	—
Total (single scan)	25	6.6	12.8	-1.7	13.3
Total (station bias)	9	6.4	8.8	-1.9	9.6





1



2

3

4

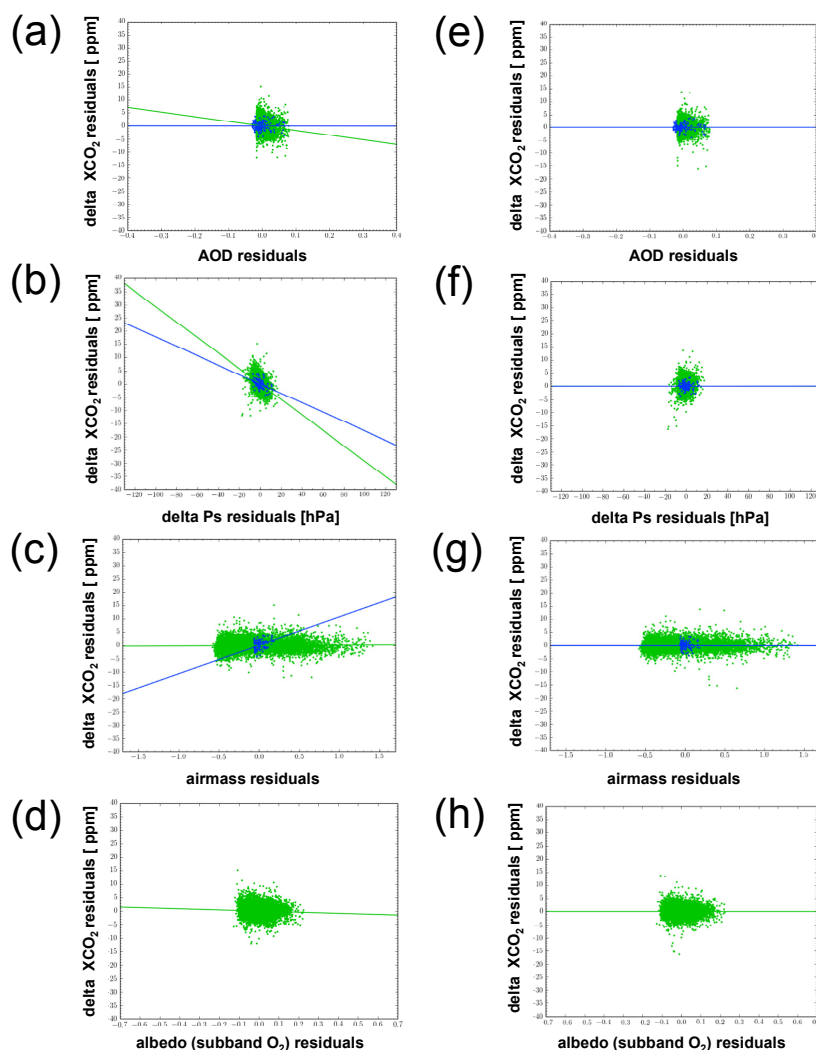
5 Fig. 1. Global distributions of (a) the TCCON sites used for correction and validation of

6 GOSAT data and (b) the aircraft observation sites used for validation of GOSAT data.

7

8

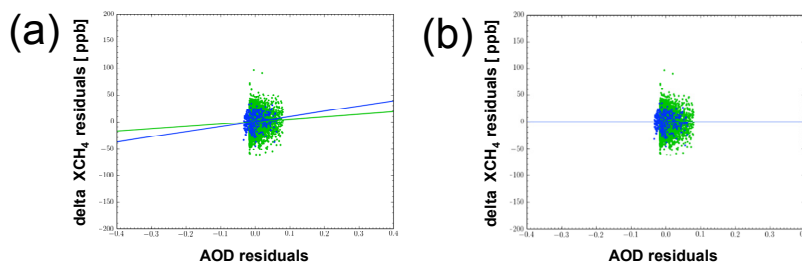
9



1

2 Fig. 2. Scatter diagrams between  $\Delta XCO_2$  calculated from uncorrected GOSAT data and (a)  
 3 the retrieved aerosol optical depth, (b) the difference between the retrieved and a priori  
 4 surface pressures, (c) airmass, and (d) surface albedo for the O<sub>2</sub> A-band. Scatter diagrams  
 5 between  $\Delta XCO_2$  calculated from corrected GOSAT data and (e) the retrieved aerosol optical  
 6 depth, (f) the difference between the retrieved and a priori surface pressures, (g) airmass, and  
 7 (h) surface albedo for the O<sub>2</sub> A-band. Green (blue) dots and lines indicate the GOSAT data  
 8 and regression lines over land (ocean) regions.

9



1

2

3 Fig. 3. Scatter diagrams between  $\Delta XCH_4$  calculated from (a) uncorrected and (b) corrected  
4 GOSAT data and the retrieved aerosol optical depth. Green (blue) dots and lines indicate the  
5 GOSAT data and the regression lines over land (ocean) regions.

6

7

8

9

10

11

12

13

14

15

16

17

18

19

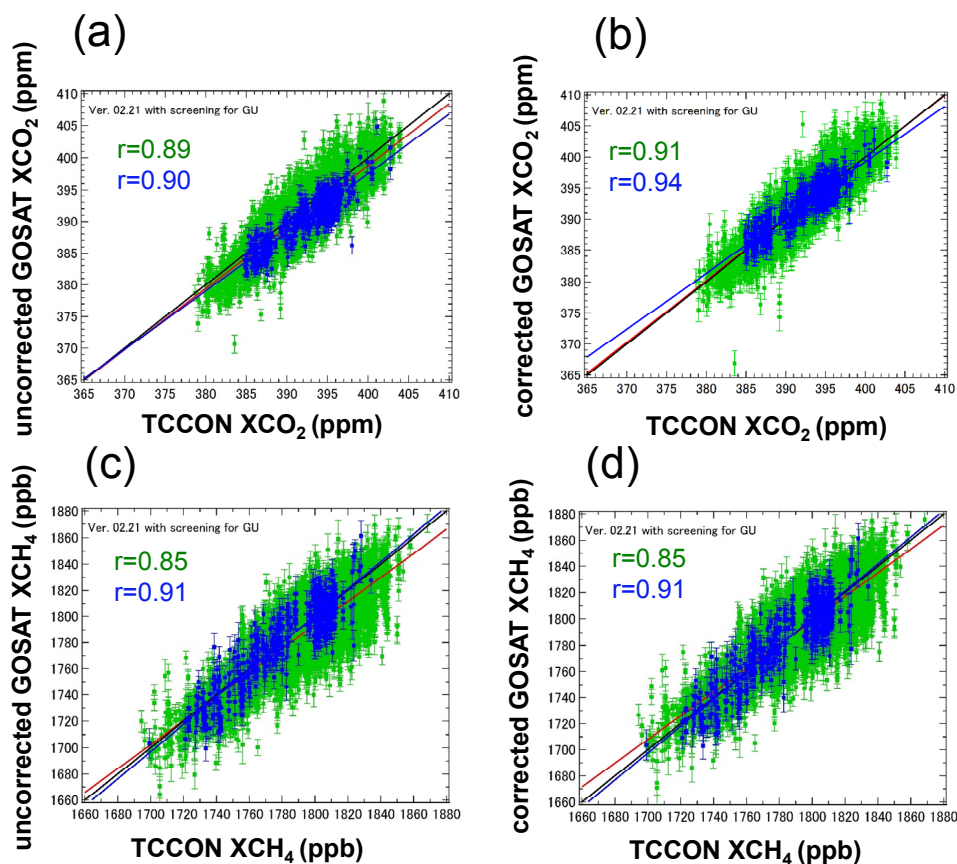
20

21



1

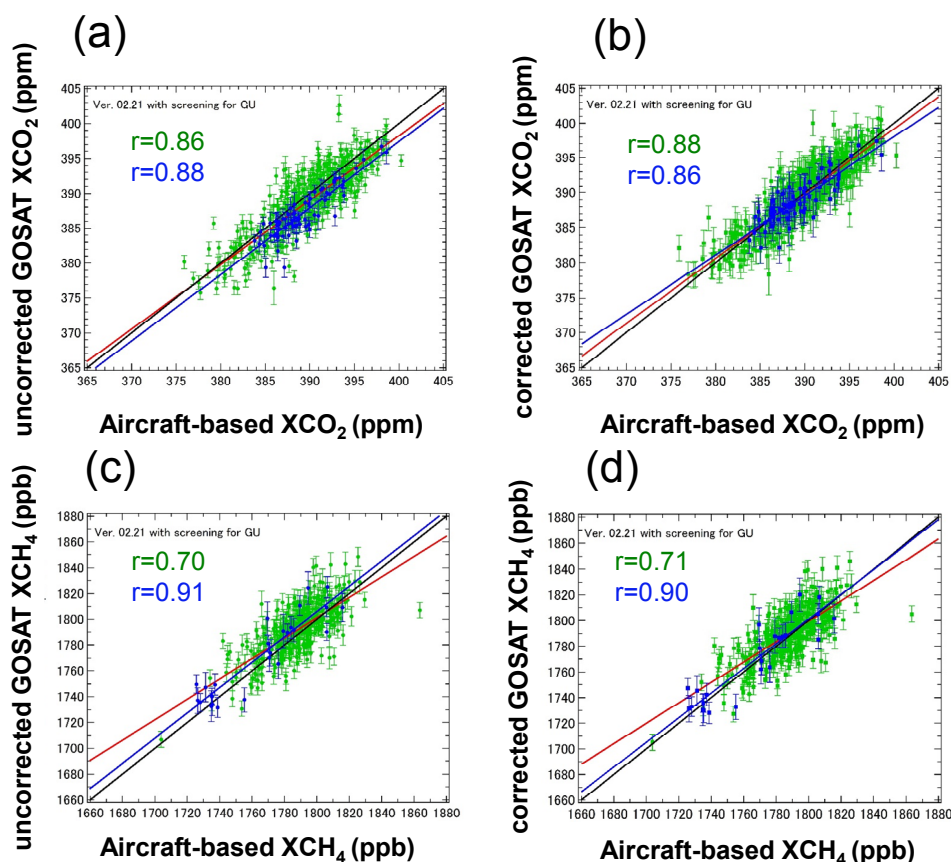
2



3

4

5 Fig. 4. Scatter diagrams between (a) uncorrected and (b) corrected GOSAT XCO<sub>2</sub> observed  
6 within ±5° latitude/longitude boxes (centered at each TCCON site) and TCCON XCO<sub>2</sub>  
7 measured on the same day. (c), (d), same as (a) and (b) for XCH<sub>4</sub>. Green and blue dots  
8 indicate GOSAT data obtained over land and ocean regions, respectively. Red and blue lines  
9 denote the regression lines, statistically significant at the 99% level, over land and ocean  
10 regions, respectively. Black lines show the one-to-one correspondence.

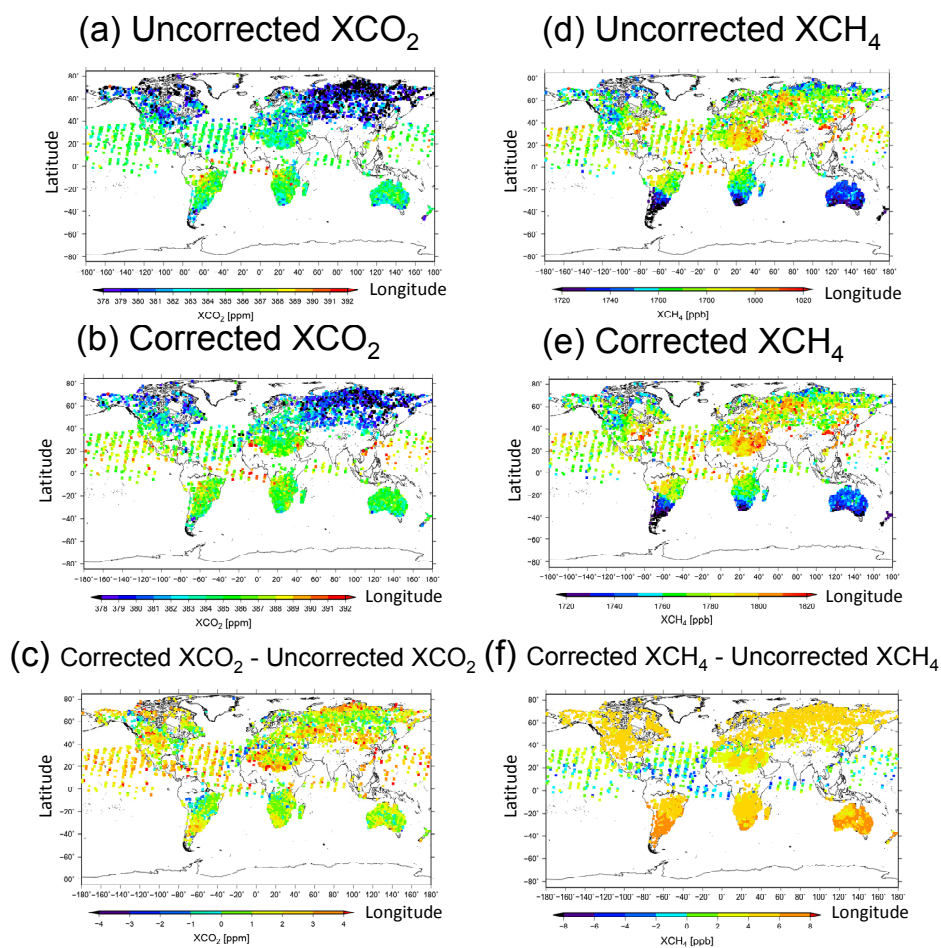


1

2

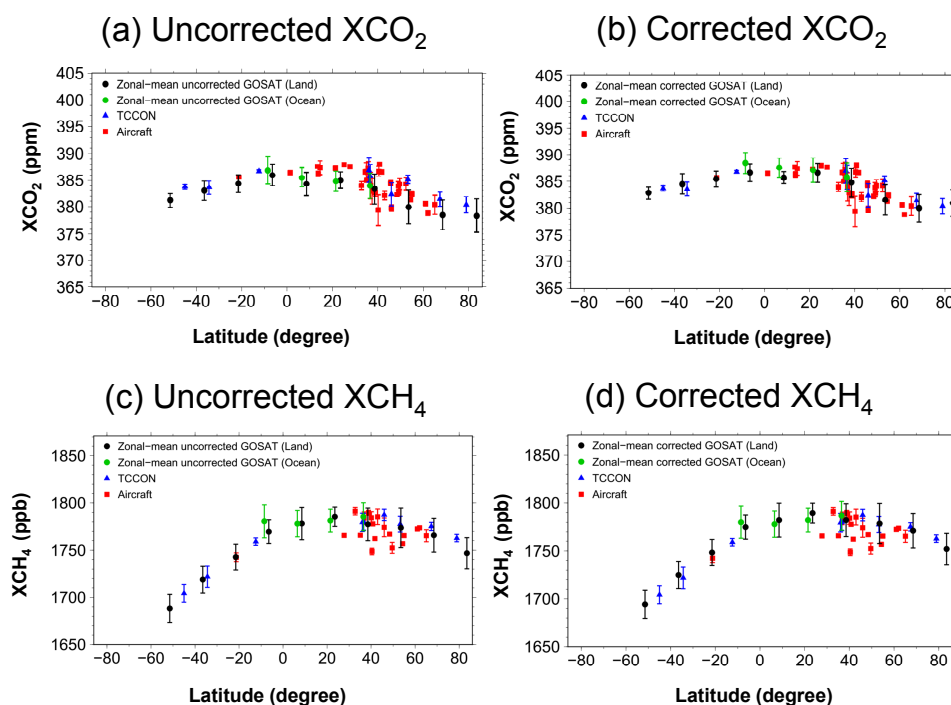
3 Fig. 5. Scatter diagrams between (a) uncorrected and (b) corrected GOSAT XCO<sub>2</sub> observed  
4 within  $\pm 5^\circ$  latitude/longitude boxes (centered on each aircraft profile) and aircraft-based  
5 XCO<sub>2</sub> observed on the same day. (c), (d), same as (a) and (b) for XCH<sub>4</sub>. Green and blue dots  
6 indicate the GOSAT data obtained over land and ocean regions, respectively. Red and blue  
7 lines denote the regression lines, statistically significant at the 99% level, over land and ocean  
8 regions, respectively. Black lines show the one-to-one correspondence.

9



1  
2  
3  
4  
5  
6  
7  
8  
9  
10

Fig. 6. Global maps of (a) uncorrected and (b) corrected GOSAT  $XCO_2$ , and (d) uncorrected and (e) corrected GOSAT  $XCH_4$  in July 2009. The differences between corrected and uncorrected (c) GOSAT  $XCO_2$  and (f) GOSAT  $XCH_4$ .



1

2

3

4 Fig. 7. Latitudinal distributions of (a) uncorrected and (b) corrected GOSAT XCO<sub>2</sub>, TCCON  
5 XCO<sub>2</sub>, and aircraft-based XCO<sub>2</sub> in July 2009. Latitudinal distributions of (c) uncorrected and  
6 (d) corrected GOSAT XCH<sub>4</sub>, TCCON XCH<sub>4</sub>, and aircraft-based XCH<sub>4</sub> in July 2009. Black  
7 and green circles indicate the zonal-mean GOSAT data retrieved over land and ocean regions,  
8 respectively. The blue triangles and red squares denote the TCCON data and aircraft-based  
9 data, respectively, at each observation site. See text for details.

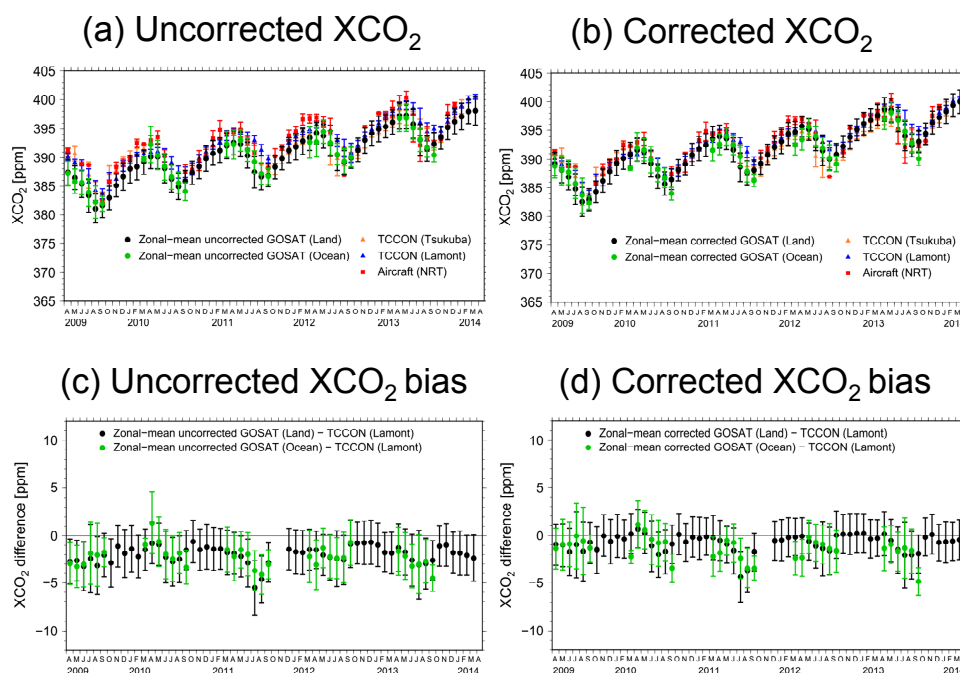
10

11

12

13

14



1

2

3

4 Fig. 8. Temporal variations of (a) uncorrected and (b) corrected GOSAT XCO<sub>2</sub>, TCCON  
 5 XCO<sub>2</sub>, and aircraft-based XCO<sub>2</sub>. Black and green circles in (a) and (b) indicate the monthly  
 6 zonal-mean GOSAT data retrieved over land and ocean regions, respectively, within a 30°–  
 7 45°N latitudinal band. The orange triangles, blue triangles, and red squares in (a) and (b)  
 8 denote the TCCON XCO<sub>2</sub> at Tsukuba and Lamont, and aircraft-based XCO<sub>2</sub> at Narita,  
 9 respectively. Temporal variations of the differences between (c) uncorrected and (d) corrected  
 10 GOSAT XCO<sub>2</sub> and TCCON XCO<sub>2</sub> at Lamont (GOSAT XCO<sub>2</sub> minus TCCON XCO<sub>2</sub>) over  
 11 land (black dots) and ocean (green dots). See text for details.

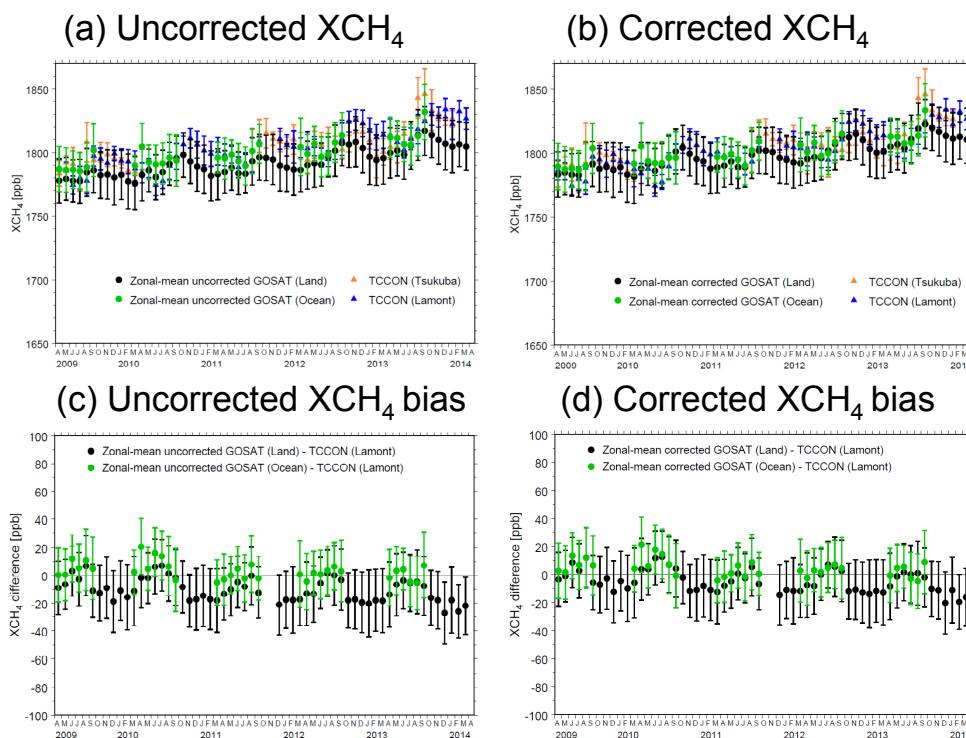
12

13

14

15





1

2

3

4 Fig. 9. Temporal variations of (a) uncorrected and (b) corrected GOSAT XCH<sub>4</sub> and TCCON  
 5 XCH<sub>4</sub>. Black and green circles in (a) and (b) indicate the monthly zonal-mean GOSAT data  
 6 retrieved over land and ocean regions within a 30°–45°N latitudinal band, respectively. The  
 7 orange and blue triangles in (a) and (b) denote the TCCON XCH<sub>4</sub> at Tsukuba and Lamont,  
 8 respectively. Temporal variations of the differences between (c) uncorrected and (d) corrected  
 9 GOSAT XCH<sub>4</sub> and TCCON XCH<sub>4</sub> at Lamont (GOSAT XCH<sub>4</sub> minus TCCON XCH<sub>4</sub>) over  
 10 land (black dots) and ocean (green dots). See text for details.